ARTICLE
https://doi.org/10.1590/2317-4889/e20250026
BJGEO Brazilian Journal of Geology

Petrographic, structural, and deformational analysis in the Curitiba Shear Zone, Ribeira Belt: a case study at São Jorge quarry, Eastern Paraná State, Brazil

Michelangelo Tissi Baldin[1]*, Eduardo Salamuni[2], Frederico Meira Faleiros[3], Leonardo Evangelista Lagoeiro[2], Emerson Sanches[2], Isonel Sandino Meneguzzo[1]

Abstract
The Ribeira Belt in southern Brazil records the Neoproterozoic tectonic evolution associated with the amalgamation of Western Gondwana, and its shear zones provide critical constraints on transcurrent–transpressive deformation regimes. Within this framework, the Atuba Complex in the Curitiba Terrane hosts the São Jorge quarry, where metatexites preserve evidence of progressive deformation. This study investigates feldspar intracrystalline plasticity and quartz–feldspar microstructures to better understand deformation mechanisms and their significance for strain partitioning during the evolution of the Curitiba Shear Zone. Petrography, structural analysis, finite strain quantification (Fry, Polar, Rf/ϕ), and electron backscatter diffraction (EBSD) were combined to characterize deformation fabrics. This research analyzes feldspar crystals to investigate intracrystalline plasticity, while finite strain quantification was primarily based on quartz grains, which serve as reliable markers for bulk strain estimates. Three deformation stages were identified: (i) ductile shear producing mylonitic metatexites with steep NE–SW foliation and sinistral kinematics, (ii) overprinting brittle–ductile deformation, and (iii) late brittle fracturing. Quartz microstructures, including lobate boundaries and grain boundary migration, indicate deformation temperatures exceeding 500°C, while feldspar exhibits undulatory extinction, subgrain formation, and moderate dynamic recrystallization. EBSD data reveal a crystallographic preferred orientation of albite consistent with {100}<010> slip, also suggesting deformation at ~500°C. Finite strain ratios are low (R ≈ 1.5-2.1), reflecting the last local increment of deformation rather than the total bulk strain, and indicating limited strain accumulation despite localized intense shearing. Brittle–ductile overprints are marked by fractures, fault zones, grain-size reduction, and comminution. Taken together, we interpret the deformation at the São Jorge quarry to be progressive, transitioning from ductile to brittle regimes within a transcurrent–transpressive setting. This interpretation provides new constraints on the structural evolution of the Atuba Complex and Curitiba Terrane and contributes to broader models of strain accommodation in the southern Ribeira Belt during the Brasiliano Orogeny.

KEYWORDS: Atuba Complex; Curitiba Terrane; shear zones; mylonites; transcurrent-transpressive regime.

1. INTRODUCTION

Rocks formed under variable metamorphic and deformational conditions, found in the internal zones of collisional orogens, show aspects of upper, middle, and lower crustal evolution, and may exhibit multiphase evolutions, contrasting metamorphic conditions, and superposition of structures (Faleiros et al., 2016).

The Ribeira Belt is characterized by products of continuous Neoproterozoic terrane interactions and is formed because of the collision between the São Francisco, Paranapanema, Luís Alves, and Congo cratons (Campanha & Brito Neves, 2004; Faleiros et al., 2011).

The Curitiba Terrane exposes part of the internal collisional zone of the southern Ribeira Belt and is in contact with the Embu and Apiaí terranes along the Lancinha-Cubatão Shear Zone (Figure 1; Faleiros, 2008, Faleiros et al., 2016).

The regional crystalline basement is cut by anastomosing shear zones, of transcurrent character and ductile or ductile-brittle nature. The deformation zones have an along-strike length of up to hundreds of kilometers and widths of up to thousands of meters. To the southwest these zones dip beneath the Paraná Basin, and to the northeast they extend offshore beneath the Atlantic Ocean (Campanha, 2002).

The Lancinha Transcurrent System comprises a set of transcurrent faults with rectilinear tracing and anastomosed aspect, including synthetic faults, antithetic faults, en échellon folds, and intrusive granites (Fiori, 1992). It is associated with the main transcurrent shear zones in the Paraná state, such as the Lancinha Shear Zone and the Morro Agudo Shear Zone (Fiori, 1985). These structures play a fundamental role in the tectonic and lithostructural compartmentalization of Precambrian terrains in Paraná State (Fiori, 1992). The basement rocks are lenticular, intensely fractured, anastomosed, and foliated, with breccias, cataclasites, sigmoidal structures, and drag folds. Brittle shear zones also display fault planes, striae, and steps. Locally, mylonites formed under ductile to ductile–brittle conditions at intermediate to deep crustal levels, where mineral stretching and flattening are well developed (Fiori et al., 1987; Fassbinder, 1990).

Ductile products of the Curitiba shear zones are rarely preserved, which often hampers detailed analysis.

[1]Universidade Estadual de Ponta Grossa – UEPG, Departamento de Geociências, Ponta Grossa, PR, Brasil. E-mails: mtbaldin@uepg.br, meneguzzo@uepg.br
[2]Universidade Federal do Paraná – UFPR, Departamento de Geologia, Curitiba, PR, Brasil. E-mails: salamuni@ufpr.br, leonardo.lagoeiro@ufpr.br, esanches.emerson@gmail.com
[3]Universidade de São Paulo – USP, Departamento de Mineralogia e Geotectônica, São Paulo, SP, Brasil. E-mail: ffalei@usp.br
*Corresponding author.

However, the protomylonitic to ultramylonitic stromatic metatexites of the São Jorge quarry display abundant planar and linear structures that provide valuable insights into these shear zones (Barros et al., 2023).

The São Jorge quarry provides an exceptional three-dimensional exposure of the Atuba Complex, where mylonitic metatexites preserve deformation structures at multiple scales. This site was chosen because it allows detailed structural analysis of the Curitiba Shear Zone (Figure 2), which is a key segment of the southern Ribeira Belt. Understanding feldspar intracrystalline plasticity in this context contributes not only to local tectonic models but also to broader interpretations of strain partitioning in orogenic transcurrent-transpressive systems.

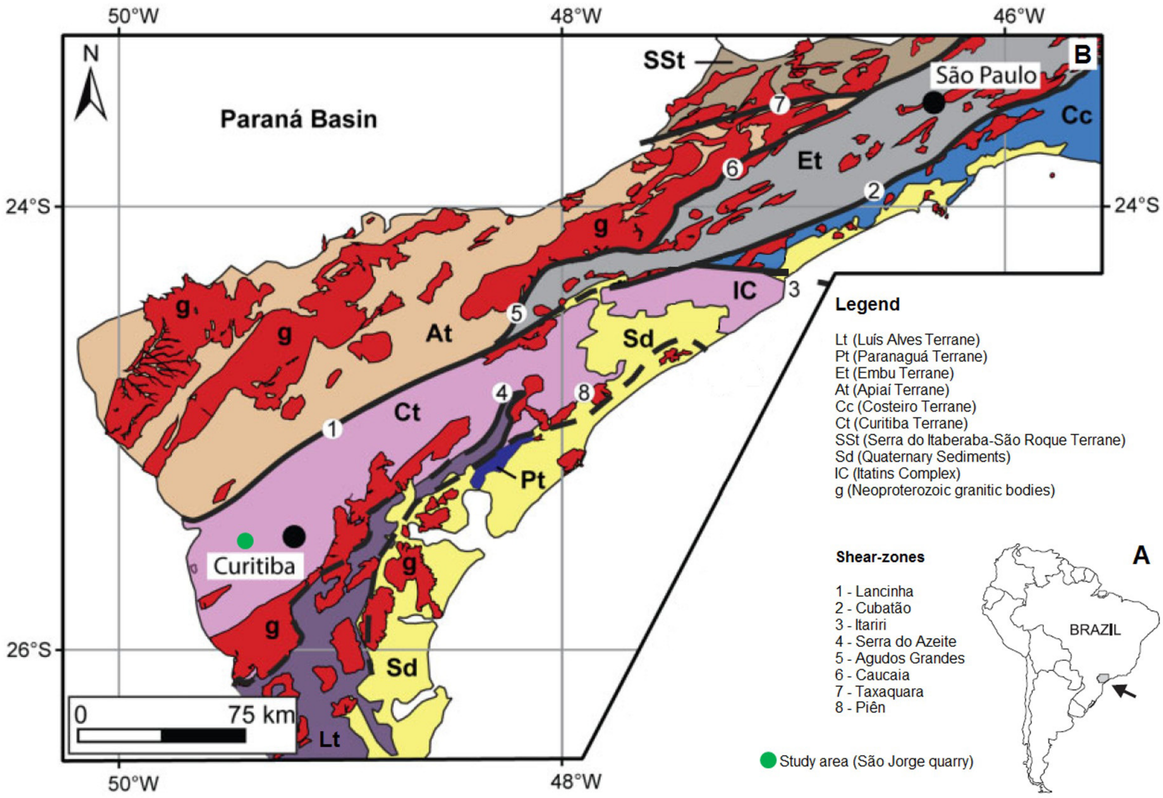

Figure 1. (A) Map of South America, highlighting the southern portion of the Ribeira Belt. (B) Study area location (São Jorge quarry), highlighted by the green circle on the map, modified from Pavan et al. (2021).

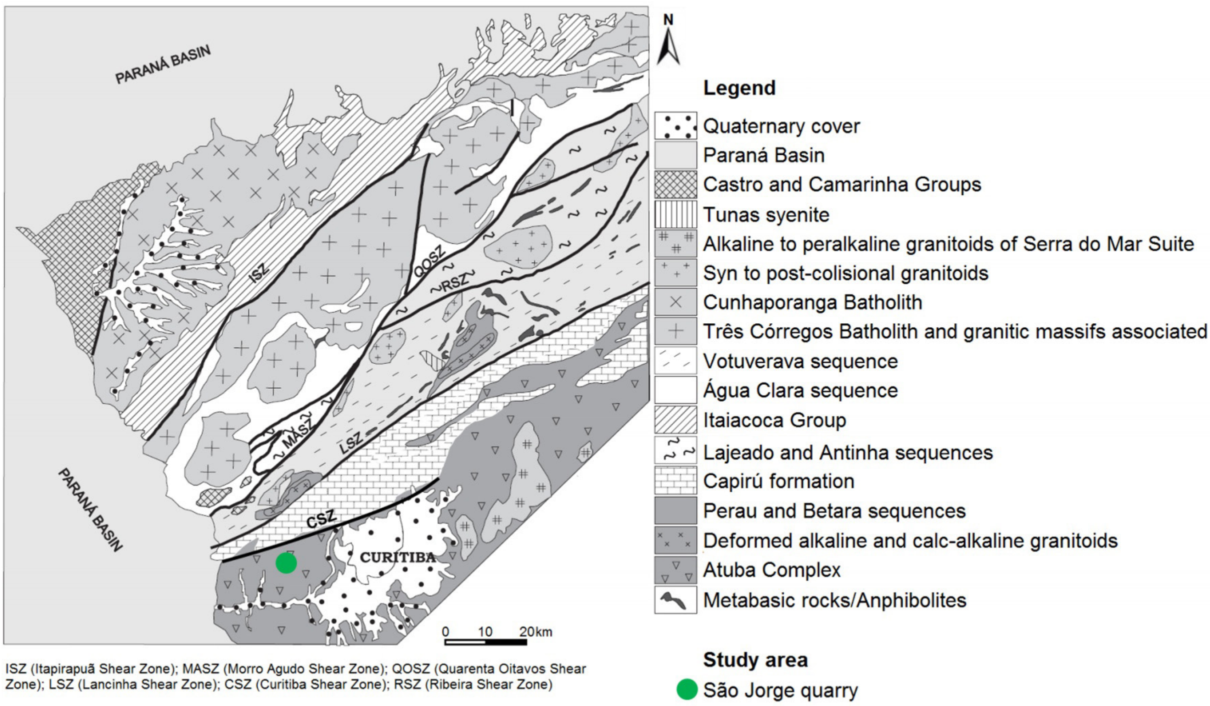

Figure 2. Geological-tectonic sketch of the Paraná State eastern portion, showing the crystalline basement and the work area in the southern direction of the map, modified from Siga Junior et al. (2003).

In this study, we investigate feldspar microstructures and crystallographic preferred orientations in the São Jorge quarry (Atuba Complex, Ribeira Belt). While quartz deformation in mylonitic rocks is well documented, feldspar behavior during ductile–brittle transitions is less understood. This provides an opportunity to evaluate deformation mechanisms in feldspar and their implications for the progressive strain history of the Curitiba Shear Zone. By combining petrographic observations, strain analysis, and EBSD, we aim to quantify finite strain and identify recrystallization mechanisms. This contributes not only to the local understanding of the Atuba Complex but also to broader discussions of intracrystalline plasticity and deformation partitioning in Neoproterozoic shear zones of the Ribeira Belt.

2. GEOLOGICAL CONTEXT

The South American Platform is composed of cratonic cores and blocks amalgamated along Neoproterozoic fold belts, and it represented a major component of the Western Gondwana supercontinent (Basei et al., 2010). The Neoproterozoic portion of the platform is divided into four major structural provinces: Borborema in the northeast, Mantiqueira in the southeast, Tocantins in the center, and Pampean in the southwest. All of them, except the Pampean Province, have been interpreted as having possible correlations with similar provinces in Africa (Basei et al., 2010).

The Mantiqueira Province extends in the NNE direction for about 3,000 km. It is a Neoproterozoic orogenic belt and occurs in Southeastern and Southern Brazil along the Atlantic coast. It is composed of several geological units with distinct ages and tectonic evolutions, including the Araçuaí, Ribeira, and Dom Feliciano belts. The terranes are separated by right-lateral transcurrent-transpressional shear zones with NE-SW directions (Brito Neves & Cordani, 1991; Heilbron et al., 2004).

The Ribeira Belt extends for 1,400 km and is between 100 and 200 km wide. It is a collisional orogenic complex, trending N60E, parallel to subparallel to the south-southeastern Brazil coast, and is related to the amalgamation of Western Gondwana (Brito Neves et al., 1999). It was deformed and metamorphosed during the Brasiliano-Pan African Orogeny. It involves Archean to Paleoproterozoic basement rocks, Mesoproterozoic, and Neoproterozoic suites of volcanosedimentary and sedimentary rocks, Neoproterozoic (Ediacaran) intrusive granitoids, passive margin sedimentary sequences and late-kinematic granites (Heilbron et al., 2004). The depositional age of many sedimentary sequences remains uncertain, with debate about their depositional environment and tectonic configuration (Campanha et al., 2008). A recent synthesis by Campanha et al. (2023) emphasizes that the southern Ribeira Belt records a polyphase evolution involving successive stages of rifting, terrane accretion, and collisional orogenesis. North of the Lancinha-Cubatão Shear Zone, the Brasiliano Orogeny is marked by 630-600 Ma granitic magmatism and Barrovian metamorphism in a subduction-to-collision setting. South of this shear zone, evidence for an early Ediacaran suture includes high-grade complexes, ultramafic suites, paired low- and high-pressure belts, and accretionary wedges with metamorphic peaks between 590-585 Ma. Subsequent terrane dispersion along strike-slip shear zones after 590 Ma produced the present-day configuration of the Ribeira Belt, with associated A-type granitic magmatism and pull-apart basins lasting into the Cambrian (500-490 Ma).

The Southern and Central Ribeira Belt is bounded to the northwest by the Paranapanema Craton, to the southwest by the Luís Alves Terrane, to the northeast by the São Francisco Craton and to the west it juxtaposes with the Brasília Belt, developing a structural, metamorphic, and geochronological interference zone. The structuring was controlled by a late transcurrent shear system of NE-SW direction, at the crustal-scale and parallel to the orogen (Campanha, 2002; Campanha & Brito Neves, 2004). The southern portion of the Ribeira Belt is divided into the Curitiba Terrane, Luís Alves Terrane, and Paranaguá Terrane. Ages range from 2.0 to 2.5 Ga, with citations for protoliths up to 3.0 Ga (Siga Junior 1995; Siga Junior et al., 1995; Sato et al., 2003).

The Curitiba Terrane is limited geologically to the northwest by the metasedimentary sequences of the Açungui and Setuva Groups, and to the southeast by the granulitic gneisses of the Luís Alves Terrane (Fuck et al., 1967; Siga Junior et al., 1995; Salamuni, 1998). One of the main boundaries between the Apiaí and Curitiba terranes was assigned to the Lancinha-Cubatão Shear Zone, which has been considered as a suture or lateral-escape zone in the Neoproterozoic (Faleiros et al., 2011). The terrane is formed by the Atuba Complex migmatites and gneisses and by the Capiru and Turvo-Cajati formations.

The Atuba Complex (Figure 2) is formed by banded migmatitic gneisses, interbedded by amphibolitic bodies, magnesian schists, and granulitic gneisses (Silva et al., 1998). It also presents paragneisses, quartzites, quartz schists, mica schists, and granitic gneisses (Siga Junior, 1995). The Capiru Formation comprises quartzites, metapelites, and marbles, and the Turvo-Cajati Formation is composed of mica schists, paragneisses, calc–silicate rocks, and marbles (Faleiros, 2008).

3. MATERIALS AND METHODS

Five field days were conducted at the São Jorge quarry for the acquisition of petrographic and structural data. The quarry exposes a large portion of the relevant rock types, allowing detailed documentation of structural features in three dimensions. Fieldwork included the systematic collection of oriented samples and structural data following the methods of Snoke et al. (1998), targeting petrographic, microtectonic, deformational, and EBSD analyses.

For the petrographic study, 20 thin sections were prepared at the Laboratory of Mineral and Rock Analysis (LAMIR, UFPR) and the Laboratory of Petrographic Lamination (LAMIN). Oriented thin sections were cut parallel to mineral lineation and perpendicular to foliation. Analyses were performed on Olympus BX60 and Leica DM 2500 P microscopes at the Didactic Microscopy Laboratory (LAPEM), with photomicrographs captured using Axio Vision software (version 4.8.2.0). Migmatites were classified according to Sawyer (2008).

Structural data were organized in Microsoft Excel (Office®) and statistically treated using Geotec Stereo software to generate Schmidt-Lambert stereograms. Paleostress analysis was carried out with the right dihedral method of Angelier & Mechler (1977) using Wintensor v. 5.8.9.

EBSD data acquisition was performed on polished thin sections prepared for feldspar crystallographic preferred orientation (CPO) analysis. Samples were polished sequentially with 3, 1, and 0.25 μm diamond pastes, followed by colloidal silica suspension to remove surface damage. Analyses were conducted on field emission gun scanning electron microscopes (FEG Quanta 450 and Tescan Mira3 LM) at the Electron Microscopy Centre (CEM) and the Materials and Structures Laboratory (LAME) of the Lactec Institute, Federal University of Paraná (UFPR), Brazil. Operating conditions included an accelerating voltage of 20 kV, a working distance of 15 mm, a specimen tilt of 70°, and step sizes ranging from 1.2 to 3.4 μm. An Oxford Nordlys Nano EBSD detector was used to acquire diffraction patterns, which were collected and indexed with the AZtec software (Oxford Instruments). EBSD data were further processed and visualized using OIM Analysis™ (EDAX) and the HKL CHANNEL 5 suite, with TANGO employed to generate misorientation histograms and MAMBO to construct pole and inverse pole figures.

Finite strain was quantified using the Fry (Fry, 1999), Rf/ϕ (Ramsay, 1967), Polar (Elliott, 1970), Flinn (1978), and Nadai–Hsü (Nadai, 1950; Hsü, 1966) methods. Recrystallized and deformed quartz grains identified in photomicrographs were used as strain markers. To characterize deformation type and intensity, one oriented thin section (cut in the XZ and YZ kinematic planes) was analyzed. EllipseFit 3.7.4 software (Vollmer, 2018) was employed for graphing and calculations, with outputs saved in Microsoft Excel (Office®).

The combination of Fry, Polar, and Rf/ϕ methods allowed the quantification of finite strain ratios, which provide insights into the magnitude and geometry of strain ellipsoids. Strain analysis based on quartz grain shapes records only the latest increment of deformation in mylonitic or strongly sheared rocks, rather than the total finite strain. Nevertheless, it remains a robust comparative tool for evaluating relative strain variations between samples (Campanha, 2002; Faleiros, 2003). EBSD analysis of feldspar was also performed because feldspar crystals, although less commonly studied than quartz, can preserve deformation mechanisms such as dislocation creep and specific slip systems (e.g., {100}<010>). This approach enables us to evaluate recrystallization processes in feldspar and compare them with quartz-based deformation estimates.

4. RESULTS

4.1 Petrography and field relations

The São Jorge quarry exposes a sequence of protomylonitic, mylonitic, and ultramylonitic stromatic metatexites. Protomylonitic bands are typically 5 m thick, with local transitions to mylonitic varieties, distinguished by finer grain size and stronger foliation. At the quarry scale, these varieties are distributed along major bands parallel to S_n foliation. The stromatic metatexites are composed of quartz-rich granodiorites and granitoids (Figure 3). Ultramylonites were also observed in ductile shear zones and granitic intrusions.

The outcrop consists predominantly of stromatic metatexites recrystallized into protomylonitic to ultramylonitic rocks, with a relatively high proportion of pinkish leucosome and subordinate white leucosome (Figure 4A). The subvertical bands of pinkish or white leucosome are mainly aligned parallel to the fine-grained mylonitic foliation, giving the outcrop a stromatic-like appearance. However, this banding likely reflects the transposition of pre-existing compositional heterogeneities rather than primary migmatitic structures. The pinkish leucosome bands (Figure 4B) are fine- to coarse-grained, with centimetric to metric thickness, and are characterized by K-feldspar, plagioclase, and quartz, interspersed with a thin, mesocratic to melanocratic residual neosome formed by plagioclase, biotite, amphibole, and quartz. The mylonitic texture is defined by rounded or elongated K-feldspar and plagioclase porphyroclasts surrounded by irregular levels of biotite or quartz-feldspathic matrix. The porphyroclasts can also occur randomly, showing no preferred direction of shape, amidst the aphanitic matrix rock. They may show centimetric sizes and low asymmetry.

White leucosome levels are millimeter- to centimeter-thick and consist of plagioclase and quartz. The leucosome domains are laterally persistent and foliated, locally situated as boudins. Many of the leucosome stromatic domains exhibit pinch-and-swell structures. The melanosome occurs at the leucosome edges, is millimeter- to centimeter-thick, and is defined by the orientation of biotite and rare amphibole crystals. Contacts between the neosome and the residual neosome are abrupt.

4.1.1 Protomylonites

The protomylonitic stromatic metatexites with granodioritic composition form regular NE–SW-trending bands in the São Jorge quarry, with thicknesses varying between 1 and 5 meters. More than one band is exposed, locally transitioning into mylonitic varieties that are distinguished by finer grain size, a higher proportion of recrystallized quartz and feldspar, and a stronger foliation. They are constituted by mineral stretching and mylonitic foliation (S_n) of penetrative character. They have a planar, lenticular, or anastomosed arrangement. The rock is fine- to medium-grained and the texture is porphyroclastic, variable with deformation intensity. The mylonitic foliation (S_n) is anastomosed and marked by quartz bands, elongated feldspars, attenuated porphyroclasts, biotite orientation, and the increase of the recrystallized matrix. The porphyroclasts are mainly oligoclase and microcline, make up 70% of the rock, and measure up to 4 mm in diameter. The recrystallized matrix is formed by quartz, oligoclase, and microcline, making up a total of 30% of the rock.

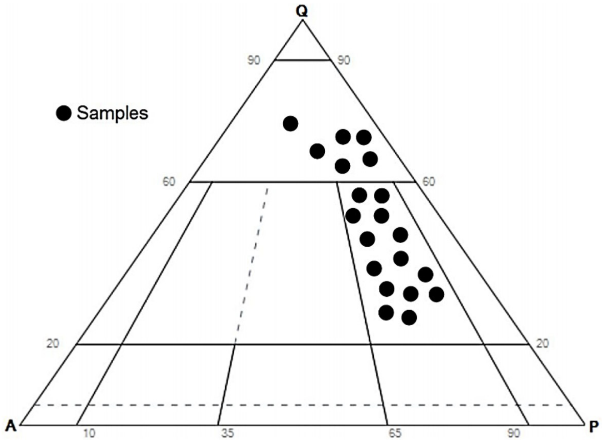

Figure 3. QAP diagram for the São Jorge quarry rocks, modified from Le Maitre et al. (2008).

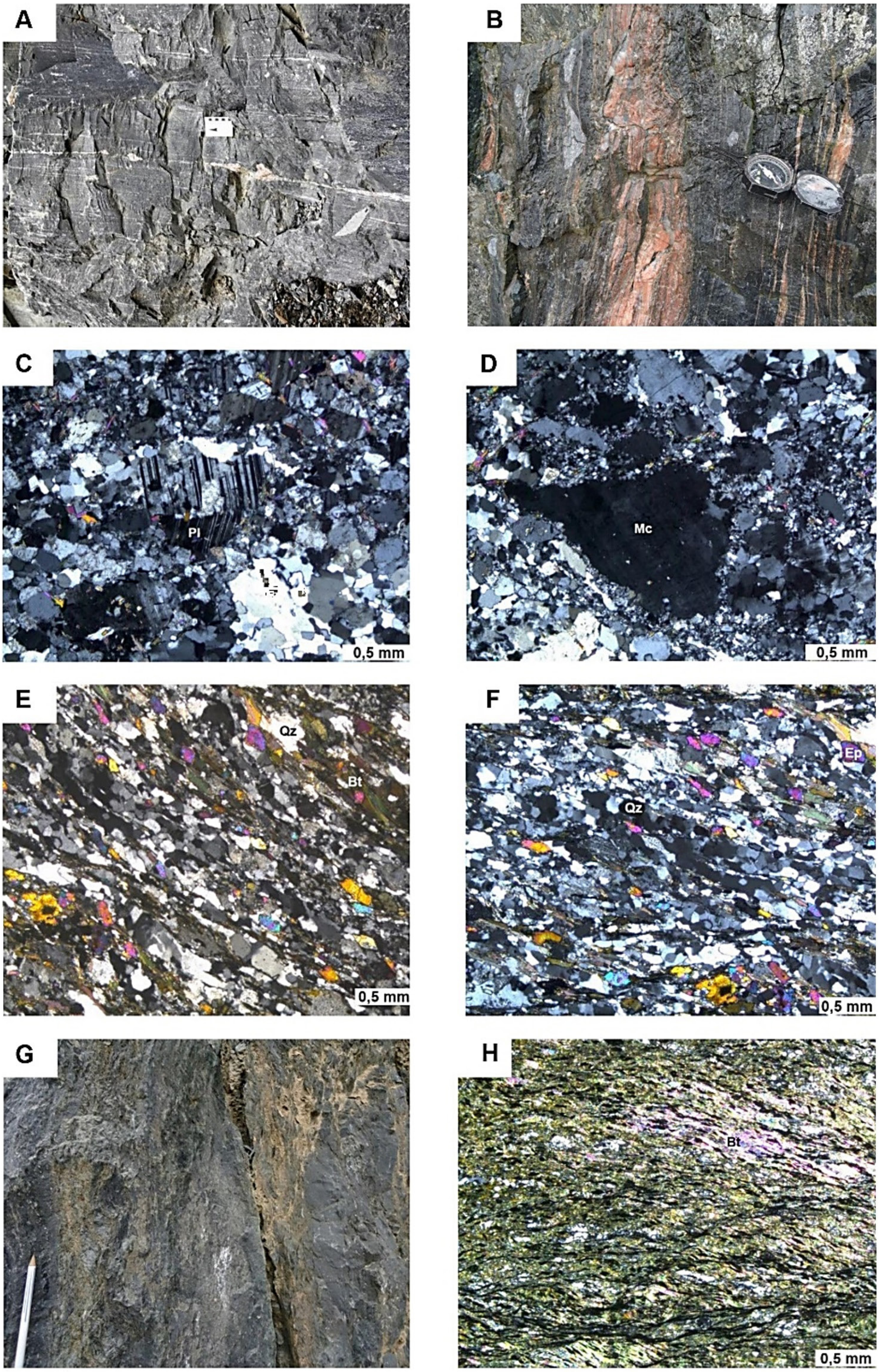

Legend: Pl - plagioclase; Qz - quartz; Bt - biotite; Ep - epidote; Ms - muscovite; Mc - microcline.

Figure 4. Field and microstructural features of stromatic metatexites from the São Jorge quarry. (A) White, millimetric- to centimetric-thick leucosome parallel to the foliation in mylonite. (B) Pinkish, centimetric, subvertical leucosome band slightly folded within ultramylonitic stromatic metatexite. (C) Oligoclase crystal showing kink-band deformation in protomylonite. (D) Microcline crystals with subgrains and new grains produced by recrystallization in protomylonite. (E) Quartz ribbon with undulatory extinction and subgrain formation in mylonite. (F) Strongly oriented quartz ribbons intercalated with biotite and epidote in mylonite. (G) Two-meter-wide ductile shear zone with ultramylonite oriented NE–SW. (H) Strongly stretched and oriented biotite crystals interspersed with quartz-rich levels in ultramylonite.

The typical mineral assemblage consists of oligoclase, quartz, muscovite, and microcline. The most common accessory minerals are biotite, apatite, opaques, and zircon. Epidote and carbonate are observed as secondary minerals. Prismatic and lamellar minerals are weakly oriented. The texture is granular, with quartz grains showing interlobate contacts.

The oligoclase crystals are thin to medium, anhedral to subhedral prismatic, and have a weak preferred orientation. The contacts are curved and serrated. They show undulatory extinction, deformational twinning, kink bands (Figure 4C), subgrains, and new grains by bulging. There is incipient saussuritization. Quartz crystals are very-fine to fine, granular anhedral, with lobated and curved contacts. There is a weak preferred orientation. They show undulatory extinction, subgrains, deformation bands, and recrystallization by grain boundary migration. The muscovite crystals are fine equigranular, subhedral lamellar and occur interstitially in the rock or oriented levels. The contacts are irregular or rectilinear. They show undulatory extinction as a deformation feature. The microcline crystals are anhedral, fine to medium, and present irregular contacts. They show optical evidence of intracrystalline deformation, such as undulatory extinction, subgrains, and moderate dynamic recrystallization (Figure 4D).

4.1.2 Mylonites

The mylonitic stromatic metatexites consisting of granodiorites and quartz-rich granitoids are characterized by regular, continuous, and relatively thick bands in the São Jorge quarry. Gradations to mylonites are observed, highlighted by reductions in grain size, mineral stretching, and strong foliation (S_n) development, evidencing a deformation of progressive and heterogeneous character. The microcline and andesine porphyroclasts have millimetric dimensions, are slightly rounded, and make up 30% of the rock. The matrix makes up 70% of the rock and is recrystallized, composed mainly of quartz, microcline, biotite, and andesine.

The average composition is quartz, andesine, muscovite, biotite, microcline, and epidote. The accessory minerals are hornblende, opaques, apatite, and zircon. Secondary minerals are carbonate, chlorite, and sericite. The texture is mylonitic, defined by quartz-feldspathic aggregates alternating with submillimetric levels of biotite and muscovite. The aggregates shape is interlobated to locally polygonal.

Quartz crystals are very-fine to medium, granular anhedral, with rectilinear and lobated contacts. They are strongly oriented. They show undulatory extinction, deformation bands, subgrains and ribbons (Figures 4E and 4F).

Andesine crystals are thin- to medium-grained, anhedral to subhedral prismatic, with serrated and indented contacts, and show weak preferred orientation. Undulatory extinction, deformational and curved twinning, albite-pericline twinning, kink bands, subgrains, and new grains formed by bulging are common; partial sericitization and saussuritization are also observed. Muscovite occurs as very-fine- to medium-grained subhedral lamellae, moderately to strongly oriented, with rectilinear contacts. It may appear slightly crenulated with biotite or outlining medium quartz grains, and typically displays undulatory extinction and curved cleavages. Biotite is very-fine- to medium-grained, anhedral to subhedral lamellar, with rectilinear to serrated contacts, strongly oriented and anastomosing. It commonly exhibits undulatory extinction and opaque inclusions, and may be altered to chlorite. Microcline is fine- to medium-grained, anhedral to subhedral prismatic, with serrated contacts, showing undulatory extinction, subgrains, and new grains. Epidote is very-fine- to fine-grained, granular anhedral to subhedral, with serrated to rectilinear contacts, typically showing undulatory extinction and moderate orientation.

4.1.3 Ultramylonites

The ultramafic stromatic metatexites occur as centimeter- to metric-thick domains or in localized ductile shear zones (Figure 4G). They have dark-gray color, granodioritic composition and are formed by biotite, quartz, plagioclase, and microcline. The accessory minerals are opaque, apatite, and zircon. The grain aggregate shape is interlobated. The minerals are strongly oriented. There is differentiated crenulation cleavage, with cleavage domains (dark, phyllosilicate-rich beds preferentially oriented) and microlithons domains formed by light quartz-rich beds moderately oriented. The foliation is micro-folded, with films of opaque minerals positioned parallel to the micro-folds' axial plane. Sub-millimetric S-C pairs consisting of opaques, micaceous minerals, and quartz levels can also be observed.

Biotite occurs as very-fine- to fine-grained, subhedral lamellae, anastomosed, strongly oriented, and stretched (Figure 4H), with rectilinear contacts, undulatory extinction, and opaque inclusions.

Quartz is very-fine- to fine-grained, granular anhedral, with serrated to rectilinear contacts, commonly showing undulatory extinction, sigmoidal shapes, ribbons, subgrains, and new grains. Quartz grains display a moderately preferred orientation and occur in aggregates of subgrains and new, slightly elongated grains arranged in anastomosed domains interspersed with biotite-rich bands. Plagioclase appears as fine-grained, anhedral crystals with serrated contacts and undulatory extinction. Microcline is also fine-grained and anhedral, with curved contacts, aligned with the S_n foliation and showing undulatory extinction together with stretching features. The ultramylonites are pinkish (Figure 5A), aphanitic rocks that exhibit intense dynamic recrystallization. They form centimeter- to meter-thick layers oriented parallel to the main foliation (S_n; Figure 5B), composed of quartz and K-feldspar with markedly diminished porphyroclasts, which are millimetric to centimetric in size and show low asymmetry.

4.1.4 Granitic intrusions

Granites occur in the northwestern portion of the main pit. They are pinkish, leucocratic, medium- to coarse-grained and isotropic. They are poorly deformed and may be boudinaged. The texture is medium- to coarse-inequigranular phaneritic. They present K-feldspar, quartz, plagioclase, and biotite. The crystals are subhedral prismatic to anhedral granular, 0.5–1.5 cm in size, and occur irregularly throughout the rock. They may show lenticular, tabular, or nearly elliptical shapes (Figure 6). The intrusions are variable in length and thickness, ranging from metric to decametric scale.

4.2 Structures and microstructures

The São Jorge quarry exhibits good rock exposures, has an approximate direction N45°E (Figure 7), and is marked by a left-lateral ductile shear zone. It is formed by a migmatite that

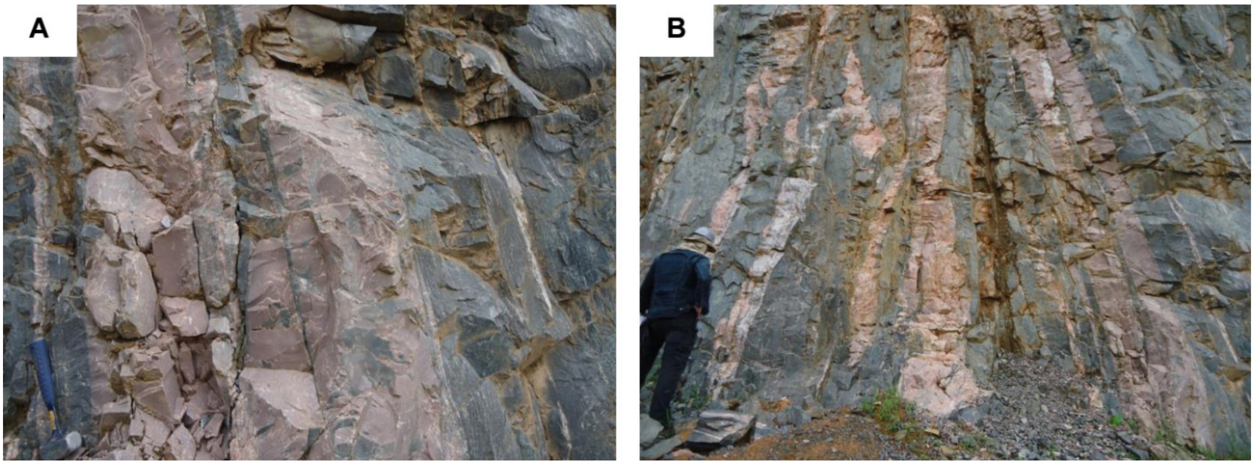

Figure 5. (A) Pink ultramylonite layer about 2 m thick. (B) Aphanitic ultramylonitic bands oriented parallel to the main foliation (S_n).

occurs frequently subvertical, has medium- to dark-gray color and fine texture, with a distinct regular, anastomosed banding, parallel to the foliation (S_n), where quartz-feldspathic bands alternate with biotite and amphibole bands.

The deformation regimes characterization in the São Jorge quarry is based on the analysis of the tectonites found, through the determination of the foliation pattern, lineations, and evaluation of the kinematic indicators. Folds, boudins, and veins can occur parallel to the mylonitic foliation (S_n). Locally an earlier foliation (S_{n-1}), crenulated and transposed by the foliation (S_n) occurs. Brittle structures such as fractures, faults, and fault striae will also be addressed with the aid of stereograms.

4.2.1 Ductile domain

The São Jorge quarry rocks present two foliations, named S_{n-1} and S_n. The surface (S_{n-1}) is poorly penetrative, local, has a low angles dip, and is marked by the orientation of biotite aggregates and stretching of plagioclase and quartz crystals (Figure 8). It is present mainly in protomylonitic rocks. It shows a ductile character, with an anastomosed and discontinuous aspect. It is affected by open to closed, millimetric to centimetric folds, with amplitude and wavelength between 1 and 2 cm. The S_{n-1} foliation exhibits a predominant NW–SE orientation, with steep dips towards either the NE or SW (Figures 9A and 9B).

The most characteristic planar structure is the protomylonitic or mylonitic (Figures 10A and 10B) foliation (S_n), marked by transposition of foliation (S_{n-1}) and partial obliteration of the compositional banding. The surface (S_n) shows a continuous, penetrative, anastomosed, or curviplanar, sigmoidal, and heterogeneous aspect, with strong parallelism, stretching, and mineral flattening. It is marked by oriented millimetric bands of quartz and biotite that outline rotated, rounded, or sigmoidal feldspar porphyroclasts. It has a general NE-SW trend and dips between 70° and 89° towards SE or NW. In some portions of the outcrop, the S-C surface of millimetric to centimetric thickness can be noted. The C' foliation was rarely observed. It has a discrete character and is oblique to the S and C surfaces. The S surface has N55E/65SE orientation, and the C surface has N55E/89SE attitude.

The S_n foliation can be defined according to Passchier & Trouw (2005) as a spaced mylonitic foliation, with an average spacing of about 10 mm. The volume percentage of cleavage is 50%. The shape of cleavage domains is rough to smooth and the spatial relation between the cleavages is anastomosed. The transition between foliation and microlithon is discrete. In the Schmidt-Lambert stereograms (Figures 10C and 10D) we see relatively high-angle dips and a concentration of poles in the SE and NW quadrants for the foliation (S_n).

Figure 6. General aspect of the granitic intrusion with an approximately elliptical shape observed at the São Jorge quarry.

The linear structures are marked by the stretching and orientation of quartz, feldspars, and biotite in the foliation plane (S_n), in addition to boudins in the leucosome, and fold axes. They have a general N40/20 and N230/10 orientation (Figure 10E). The sigmoids (Figure 11) observed in the quarry have a general direction N235/15 or N40/31.

The leucosome bands are continuous and regular, however, the leucosome can become lenticular and discontinuous by boudinage (Figures 12A and 12B) or pinch-and-swell type structures, due to the contrast in competence relative to the residual neosome.

The foliation is often affected by syn-shear folds (Figure 13A), open to closed (Figure 13B) at different scales, asymmetric, with moderate amplitude and wavelength. The limbs have general attitudes N27E/45SE and N37E/60NW. The axis direction is N220/18 or N50/11. Shear-folds are centimetric to metric (Figure 13C), with thick hinges and thinned limbs. They mainly involve the leucosome and the residual neosome (Figure 13D).

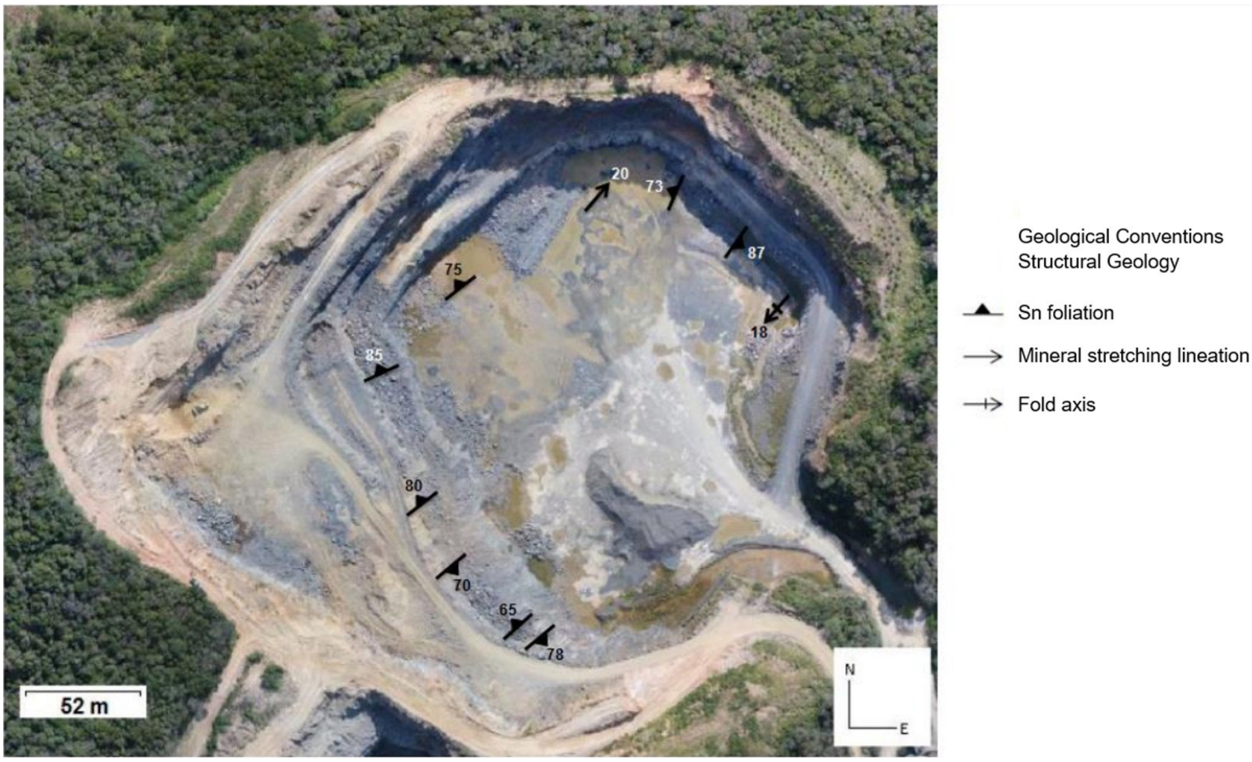

Figure 7. Main pit of the São Jorge quarry showing foliation and lineation measurements, modified from Saque (2017).

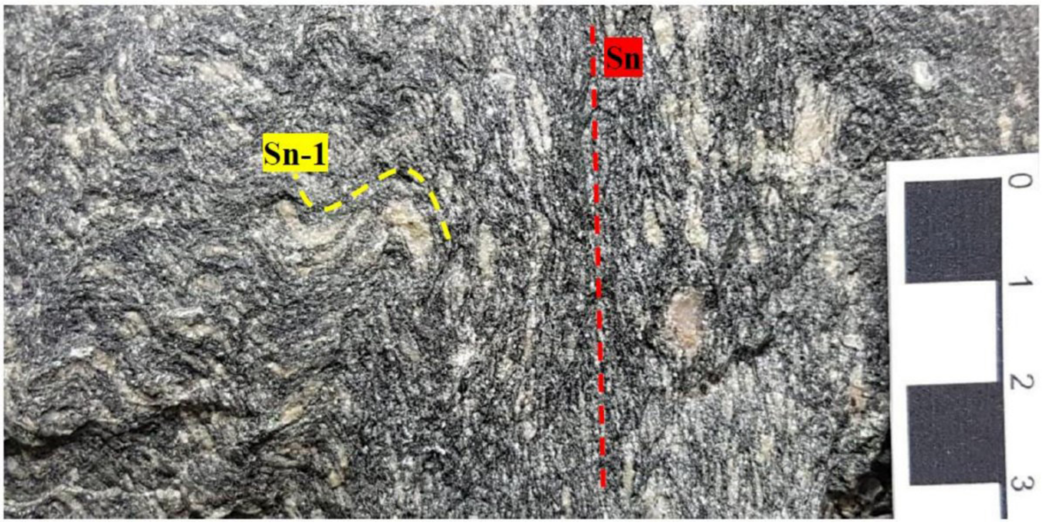

Figure 8. Foliation (S_{n-1}) is crenulated and transposed by foliation (S_n).

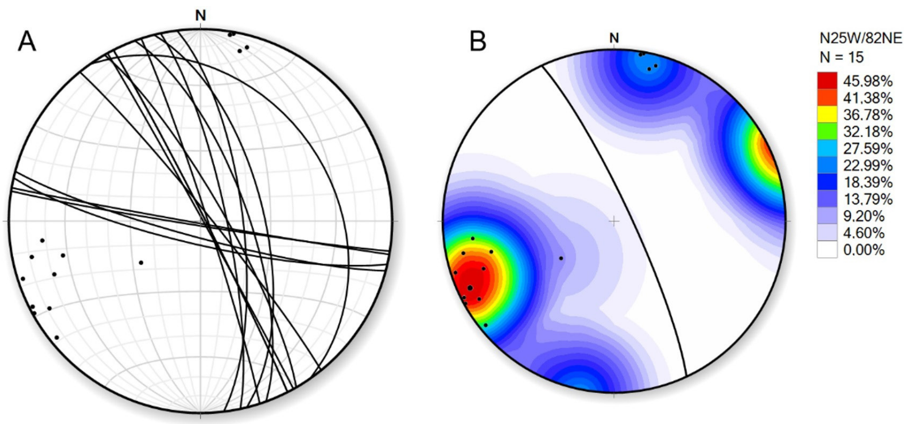

Figure 9. Structural diagrams of the São Jorge quarry rocks showing the S_{n-1} foliation: (A) Stereographic projection of the foliation planes with their poles. (B) Contour diagram of the maximum pole density.

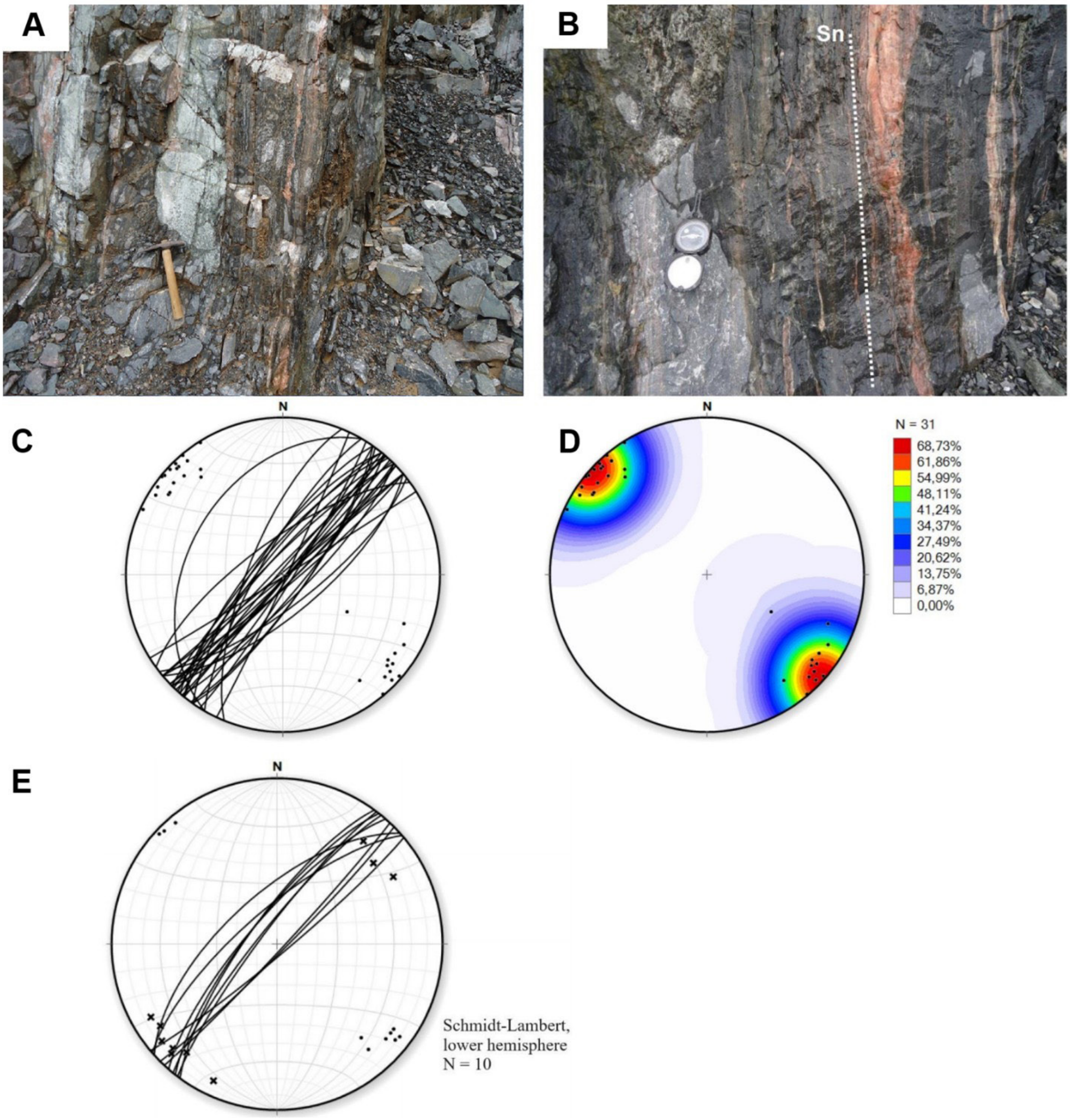

Figure 10. (A) Mylonite from the São Jorge quarry with well-developed foliation, characterized by elongated feldspar porphyroclasts set in a recrystallized quartz-feldspar matrix. The foliation strikes NE-SW and dips steeply (subvertical) to the NW. (B) General aspect of the São Jorge quarry mylonitic foliation. Structural diagrams of the São Jorge quarry rocks foliation (S_n): (C) Cyclographic representation of the planes with their poles. (D) Maximum pole contour diagram. (E) Stereogram of the São Jorge quarry showing planes and poles with their corresponding lineations.

Figure 11. Sigmoidal structures indicated by yellow arrows, formed by pink leucosome bands of centimetric to metric scale.

Laterally, the progressive increase of deformation is observed, defined by the reduction of crystal size, and increase of matrix, evidenced by the gradation of protomylonites, mylonites and ultramylonites.

Ultramylonites can occur crenulated, with submillimetric axes and millimetric wavelengths (Figure 14A). The folds have N195/12 and N50/11 axes. Microscopically, the S-C pair, quartz ribbons, and strongly oriented and microcrenulated micaceous levels are noted (Figure 14B).

Kinematic indicators such as macroscopic sigmoids of K-feldspar (Figure 15A) and plagioclase (Figure 15B), oblique foliation (Figure 15C), and quartz-feldspar aggregates (Figure 15D) suggest left-lateral movement to foliation (S_n). Macroscopic (Figure 16A) and microscopic shear bands (S-C structures; Figures 16B and 16C) indicating left-lateral direction were also observed.

4.2.2 Brittle-ductile domain

Brittle-ductile deformations are impressed in the São Jorge quarry and show planar and linear features. They were generated in a progressive shear regime and have a general NE-SW direction with high-angle dips (Figures 17A, 17B, 17C).

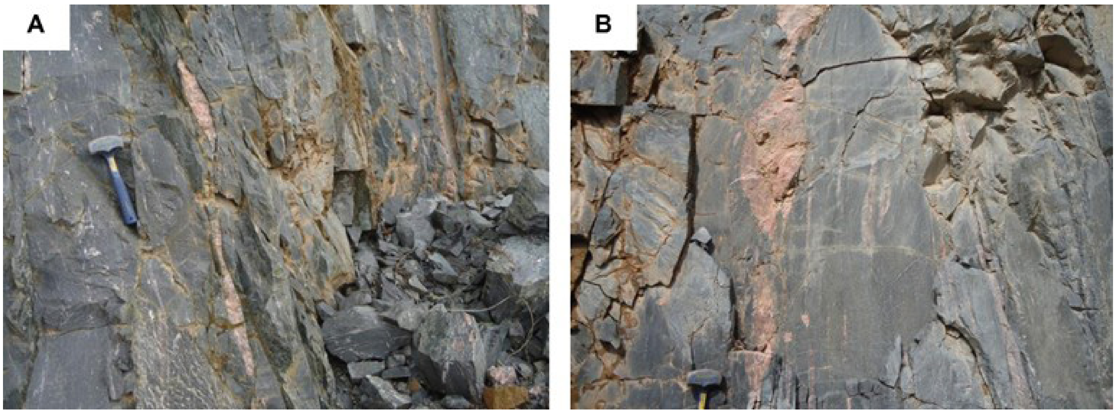

Figure 12. (A) Pink leucosome with centimetric thickness and boudinaged aspect exposed on a vertical wall. (B) Pink, metric-scale lenticular boudins within the residual neosome in a vertical exposure.

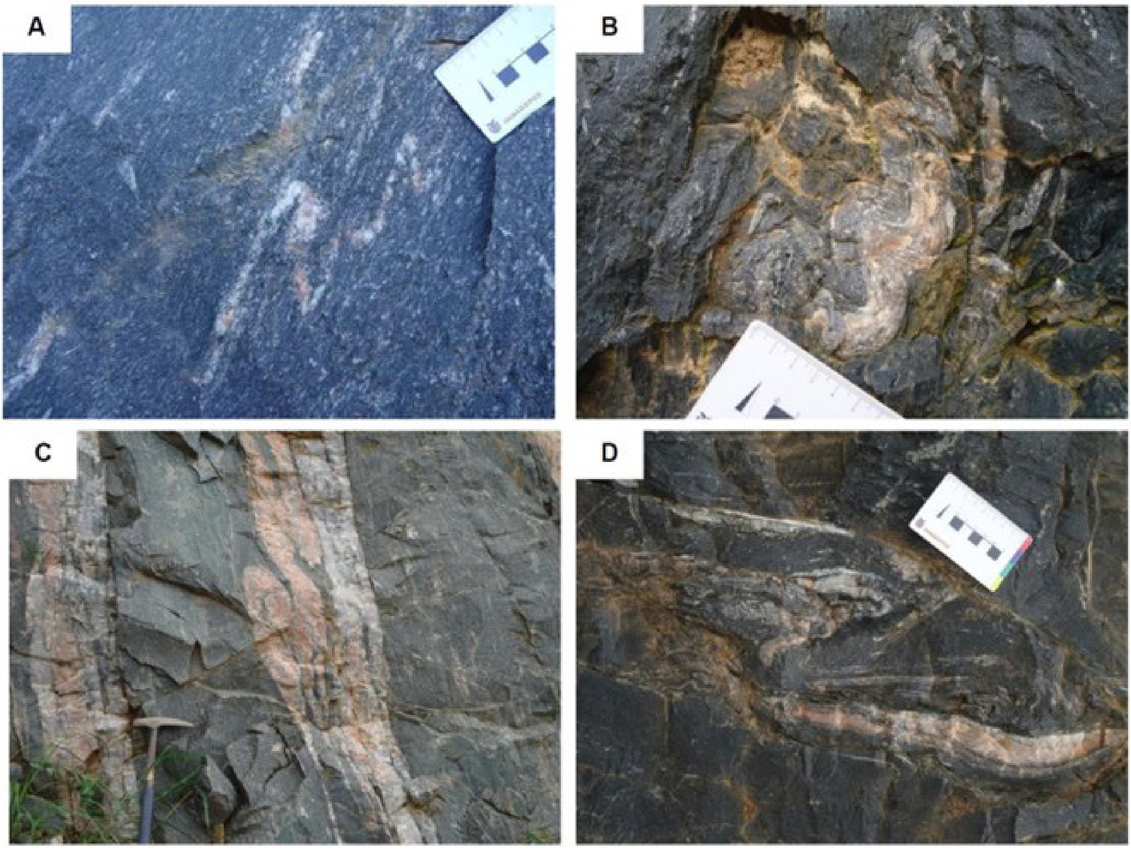

Figure 13. (A) Centimetric, asymmetric shear-folds, with varied opening angles. (B) Tight to close folds in mylonitic stromatic metatexite. (C) Shear-folds in pinkish leucosome. (D) Shear-folds involving leucosome and residual neosome.

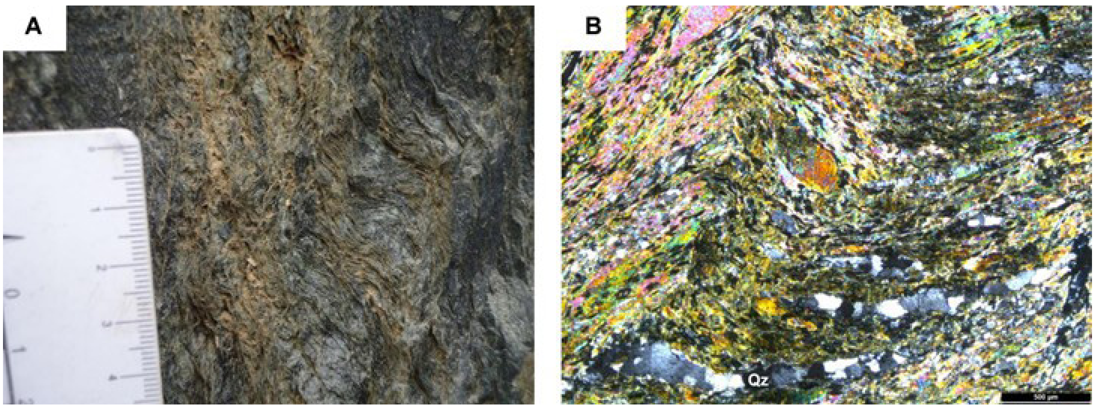

Figure 14. (A) Crenulation and S-C pair in ultramylonitic migmatite from a ductile shear zone. (B) Quartz ribbons interlayered with microcrenulated phyllosilicate levels (crossed polars). Legend: Qz – quartz.

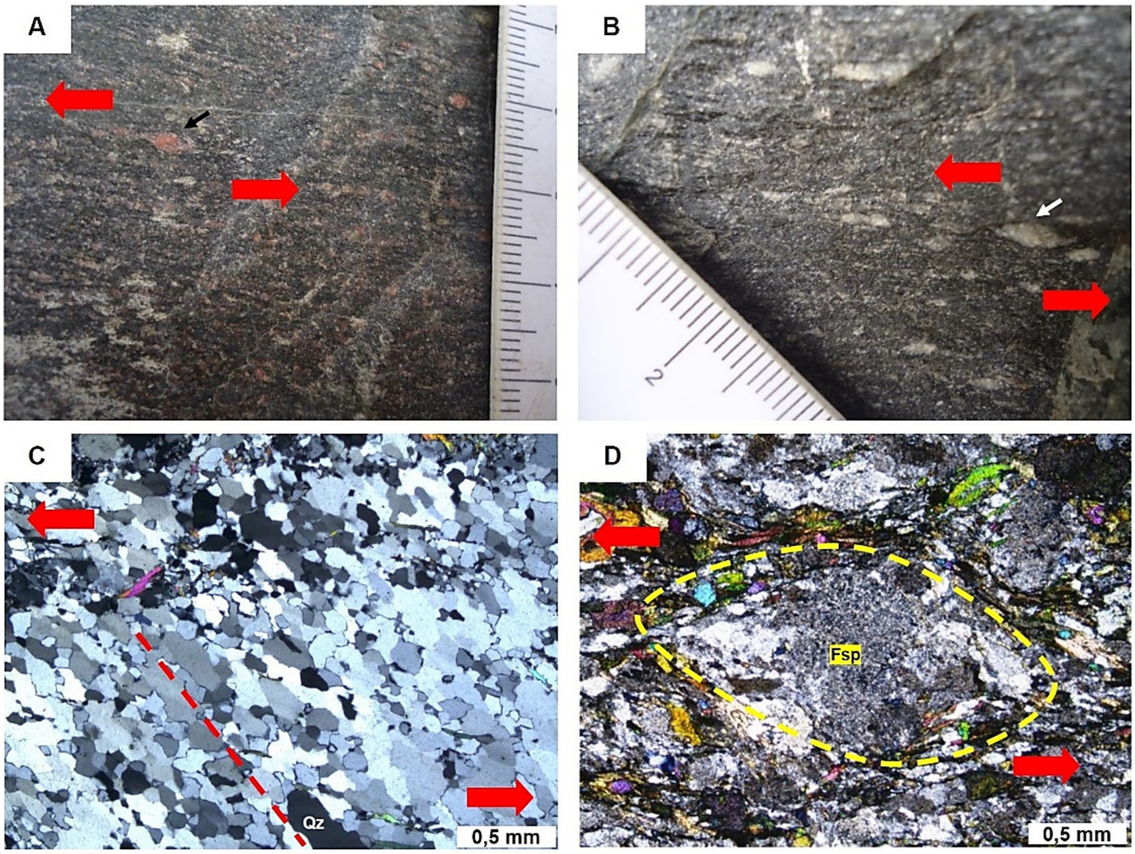

Legend: Qz - quartz. Fsp - feldspar.

Figure 15. Kinematic indicators for foliation (S_n). All features suggest left-lateral kinematics. (A) K-feldspar sigmoid indicated by black arrow. (B) Plagioclase sigmoid indicated by white arrow. (C) Oblique foliation formed by quartz grains of elongate character. (D) Quartz-feldspathic aggregates with sigmoidal shape in mylonite. Legend: Qz - quartz. Fsp - feldspar.

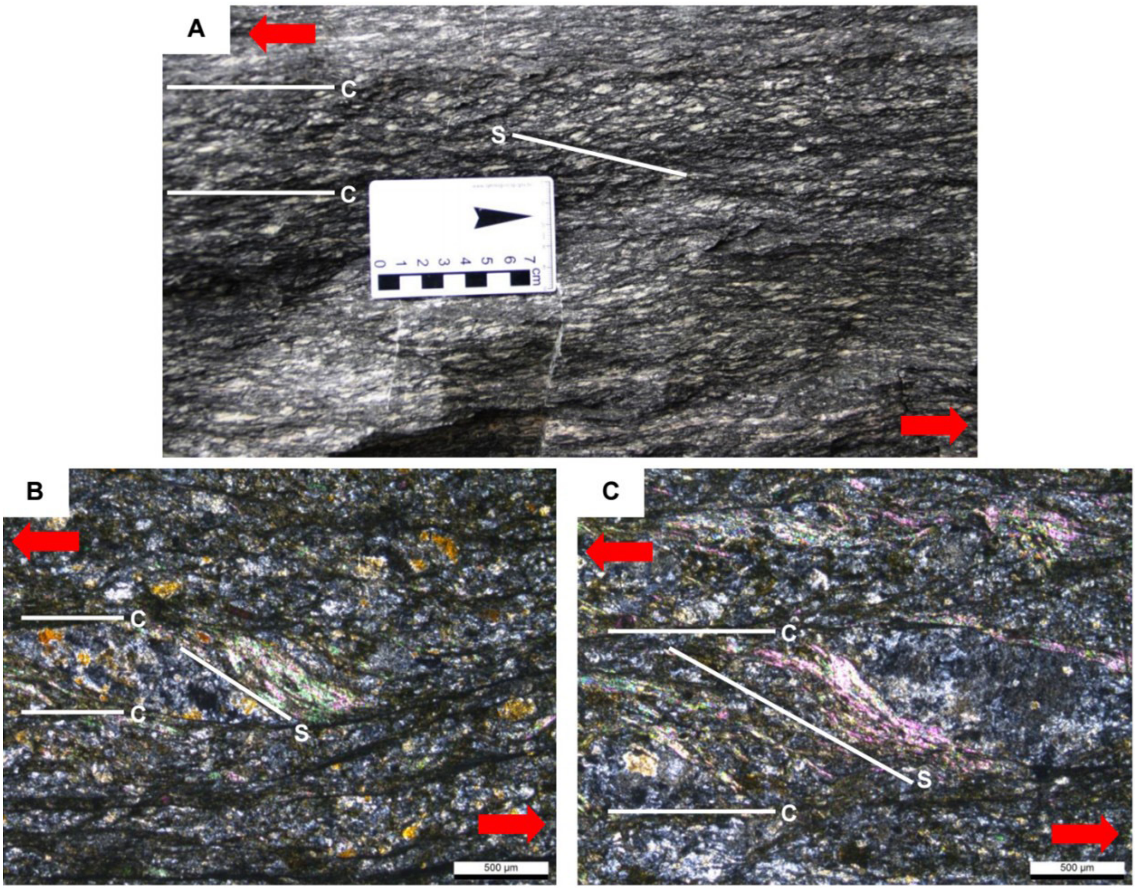

Figure 16. (A) Protomylonite with S-C structure pointing to left-lateral movement. (B) S-C pair in ultramylonite with left-lateral orientation to foliation (S_n). (C) Ultramylonite formed by shear banding, suggesting left-lateral kinematics.

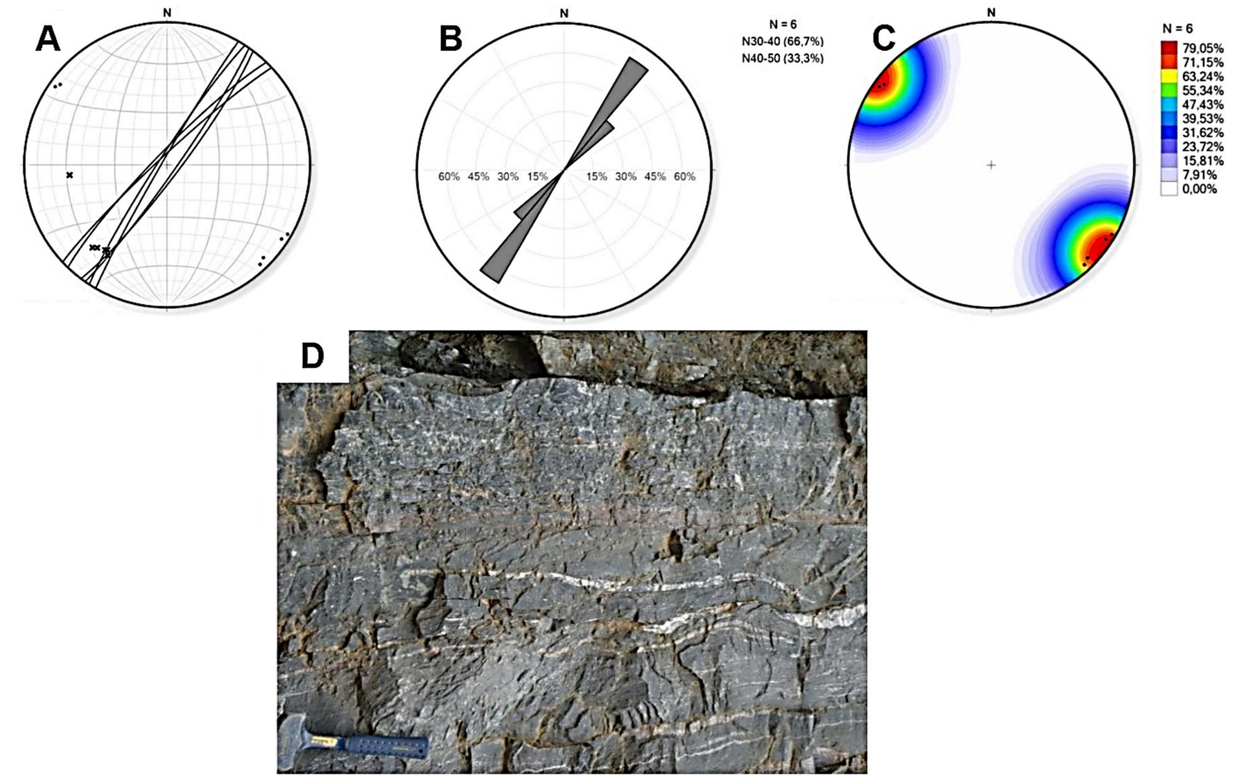

Figure 17. Structural diagrams of brittle-ductile features observed at the São Jorge quarry. (A) Cyclographic representation of the planes with their poles and striae. (B) Rose diagram. (C) Maximum pole contour diagram. (D) White, millimeter-thick, folded, and fractured quartz veins.

The shear zone is characterized by coexisting fractures and ductile deformation structures, and shows a preferred left-lateral movement sense. At these locations, the rocks show protomylonitic to mylonitic textures, broken folds, and folded, fractured, and faulted quartz veins (Figure 17D).

4.2.3 Brittle domain

Lineaments are linear or slightly curved and represent faults, fractures, shear zones, and areas of weakness in rocks (Figure 18). The São Jorge quarry has directional, diagonal, and subhorizontal fractures (Figure 19A), which can be smooth to rough, parallel, planar, sparsely- to very-dense, and metric-scaled. They are unfilled or occasionally filled with carbonate. The planes openness is centimetric, around 2 cm. There may be tight discontinuities. Persistence is low to medium. Fractures are often subparallel or parallel to the foliation (S_n; Figure19B). Locally, centimetric- to metric-scale conjugate fractures are observed (Figure 19C). Brittle shear zones may occur (Figure 19D), with the generation of cataclasites, showing evidence of comminution, generalized fracturing, and angular and polycrystalline fragments of various sizes. Schmidt-Lambert diagrams (Figures 19E and 19F) made for the fractures allowed the identification of two preferred direction families: NW-SE (Figure 20A) and NE-SW (Figure 20B).

The faults observed at the São Jorge quarry can be divided into two main sets, distinguished by cross-cutting and abutting relationships. The first and older set is associated with left-lateral transcurrent faults, while the second and younger set corresponds to right-lateral transcurrent faults, which locally overprint and displace the former. In addition, subordinate transcurrent faults with an oblique-normal component were identified.

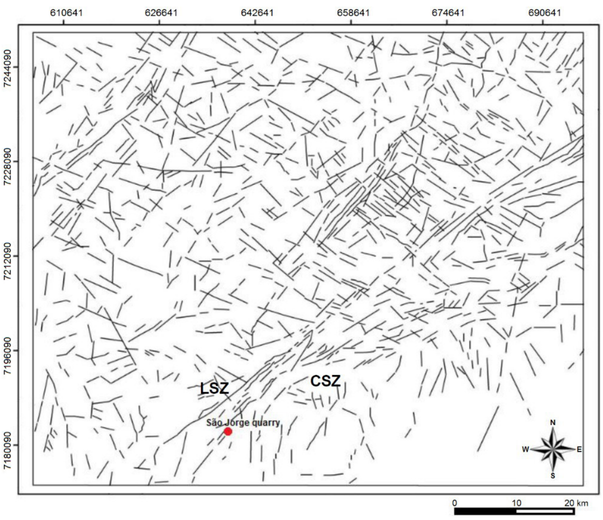

Figure 18. Tracings of the structural lineaments on SRTM digital surface terrain. Note the inflection point of the Curitiba Shear Zone (CSZ) and the Lancinha Shear Zone (LSZ) near the working área, modified from Pierin et al. (2008).

The left-lateral faults occur as metric- to decametric-scale planes, generally planar to curviplanar, with penetrative character and irregular carbonate coatings. Their average orientation is N40E/75NW. Conjugate fault sets are present and better described as R- and R'-type Riedel fractures, given their geometry relative to the inferred shear zone. Kinematic indicators such as fault striae, steps, and spoon-like features suggest sinistral motion, although many of these features are partially obliterated by subsequent dextral reactivation. Schmidt-Lambert diagrams for this generation are shown in Figures 21A, 21B, 21C.

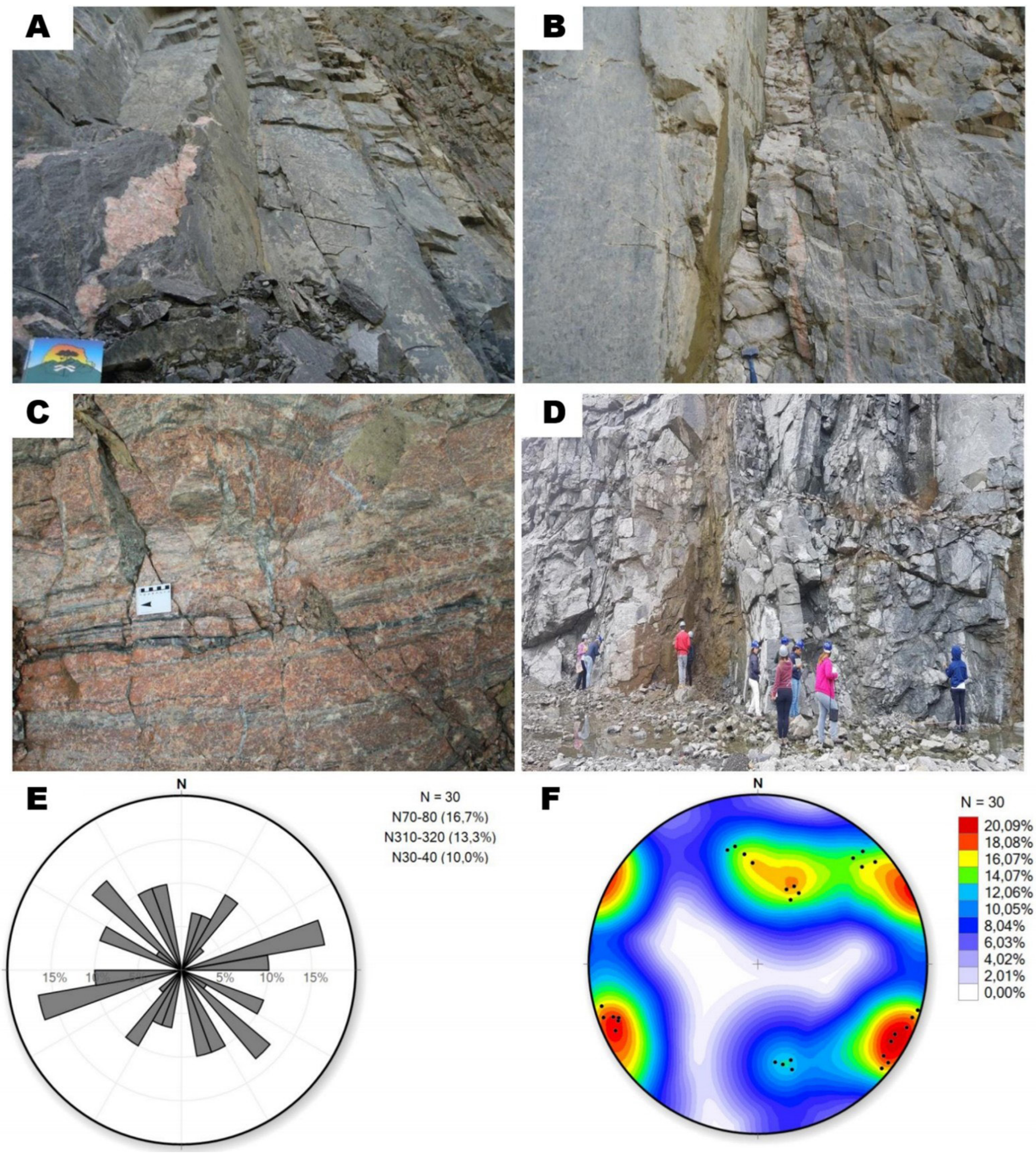

Figure 19. (A) Three fracture sets observed at the quarry wall: two subvertical and nearly orthogonal to each other, and one subhorizontal set visible on the left side. Fractures are rectilinear and lack mineral filling. (B) Vertical NE-SW-oriented planes, parallel to subparallel to the mylonitic foliation (S_n). (C) Conjugate centimetric fractures in mylonites bands. (D) Decametric-thick brittle shear zone, formed by subvertical and oblique fractures, parallel to each other and with planar geometry. Structural fracture diagrams for the São Jorge quarry rocks. (E) Rose diagram. (F) Maximum pole contour diagram.

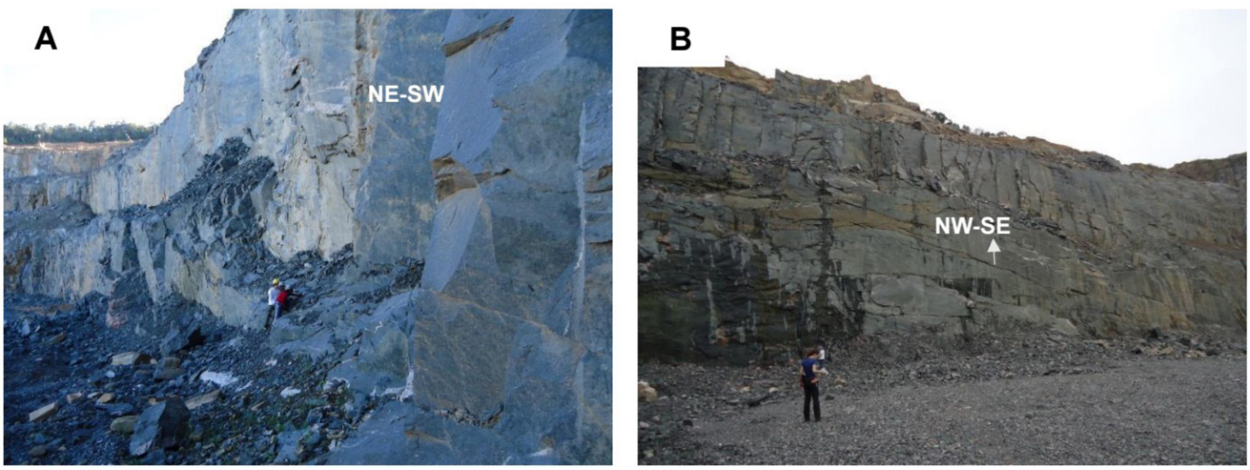

Figure 20. Fracture sets in the São Jorge quarry. (A) Subvertical fractures striking NE-SW. (B) Inclined fractures striking NW-SE. These fracture systems overprint the mylonitic foliation and represent late brittle structures.

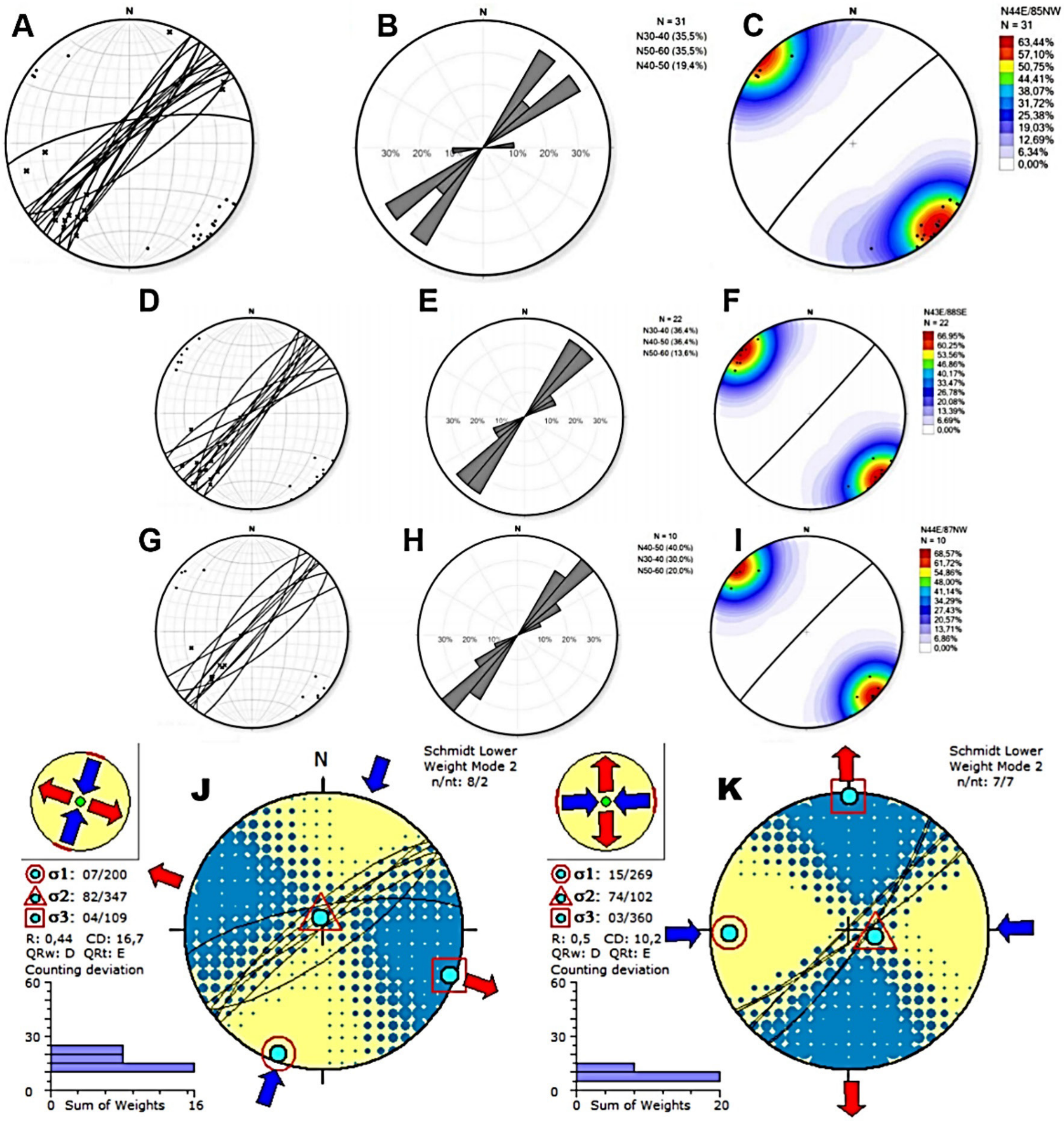

Figure 21. Structural diagrams of the left-lateral transcurrent faults. (A) Cyclographic representation of the planes with their poles and fault striae. (B) Rose diagram. (C) Contour diagram of maximum poles. Structural diagrams of the right-lateral transcurrent faults. (D) Cyclographic representation of the planes with their fault poles and striae. (E) Rose diagram. (F) Contour diagram of maximum poles. Structural diagrams of transcurrent faults with a normal component. (G) Cyclographic representation of the planes with their poles and fault striae. (H) Rose diagram. (I) Contour diagram of maximum poles. Paleostress diagrams of the São Jorge quarry transcurrent faults. (J) Left-lateral faults. (K) Right-lateral faults.

The right-lateral transcurrent faults strike the NE-SW direction with a high-angle dip. They occur systematically along the quarry, with the generation of kinematic indicators such as fault striae and centimetric steps. The planes are metric to decametric, parallel to subparallel, curviplanar, smooth, penetrative, and directional, and may be filled by carbonates. Spacing varies from sparsely dense to dense and there is no alteration of the walls. There are dark gray fault mirrors formed predominantly by biotite, with dimensions around 15 m. Locally, en échelon fractures occur. Schmidt-Lambert diagrams are shown in Figures 21D, 21E, 21F.

The transcurrent faults with normal components have little representation in the outcrops examined. The planes are poorly penetrative, sparse, and slightly oblique. The Y-fault presents general direction N45E/80NW or N40E/78SE. The fault planes are formed by centimetric steps and slickensides, with medium angle dip towards SW. Schmidt-Lambert diagrams are seen in Figures 21G, 21H, 21I.

Paleostress inversion (Figures 21J, 21K) of the structural data indicates that the left-lateral faults developed under a stress field with σ1 oriented approximately N20E, vertical σ2, and σ3 trending N70W. In contrast, the right-lateral faults formed under a regime characterized by an E–W oriented σ1, a N–S σ3, and subvertical σ2.

There are white-colored, rarely zoned, mylonitized, weakly to strongly fractured quartz veins, ranging in thickness from 0.1 to 50 cm (Figure 22A). They occur parallel to the mylonitic migmatites foliation (S_n; Figure 22B). They may be foliated (Figure 22C) and affected by open (Figure 22D) to closed centimetric folds. Sigmoidal veins (Figure 22E) and shear-folds (Figure 22F) also occur. The attitudes are depicted in Figures 23A, 23B. Microscopically the quartz crystals are fine to medium, granular anhedral, with serrated, amoeboid (Figure 24A) and curved contacts. They show subgrains, stretching (Figure 24B), and undulatory extinction.

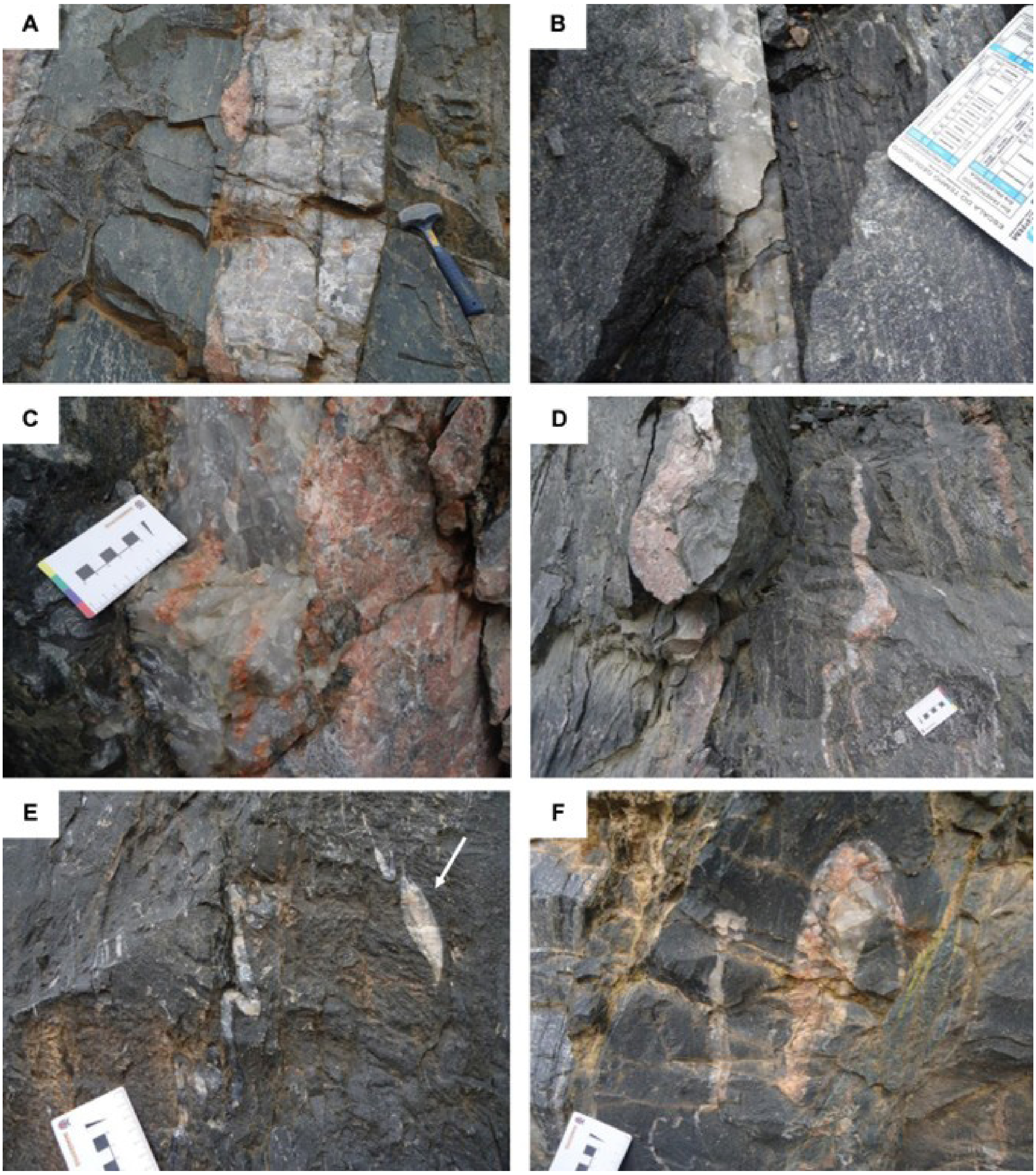

Figure 22. (A) Quartz vein ~50 cm thick with overall orientation N40E/80NW. (B) Quartz vein parallel to foliation (S_n). (C) Foliated quartz vein. (D) Quartz vein showing open folds. (E) Sigmoidal geometry of the quartz vein (indicated by the white arrow). (F) Shear folds affecting the quartz vein.

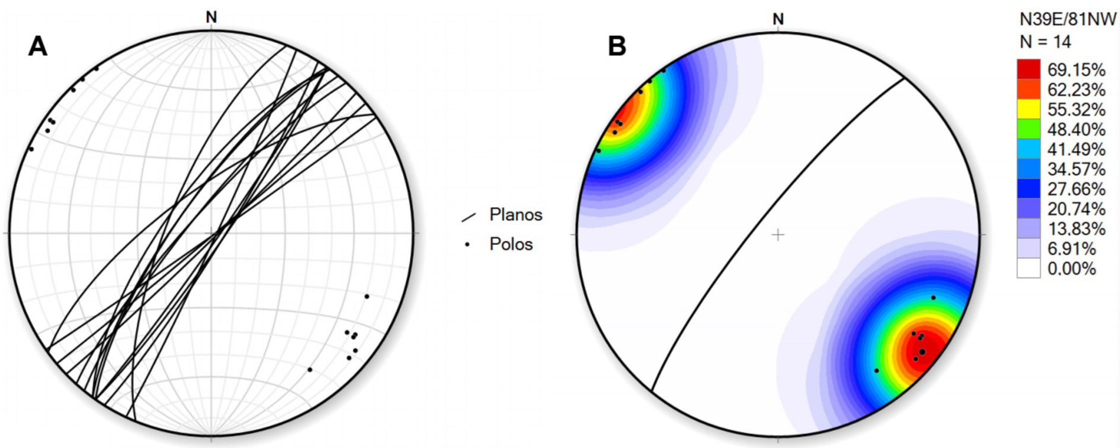

Figure 23. Structural diagrams of quartz veins. (A) Cyclographic representation of planes with their poles. (B) Pole density contours. The maximum plane is N39E/81NW. Schmidt-Lambert, lower hemisphere. N = 14.

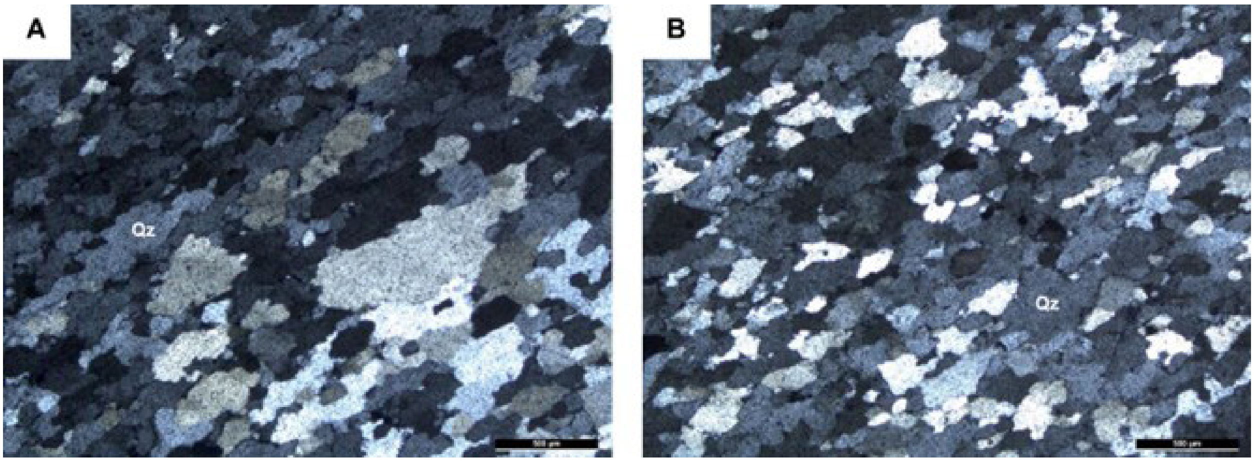

Figure 24. (A) Amoeboid texture of quartz (cross-polarized light). (B) Oriented and elongated quartz grains (cross-polarized light). **Legend:** Qz – quartz.

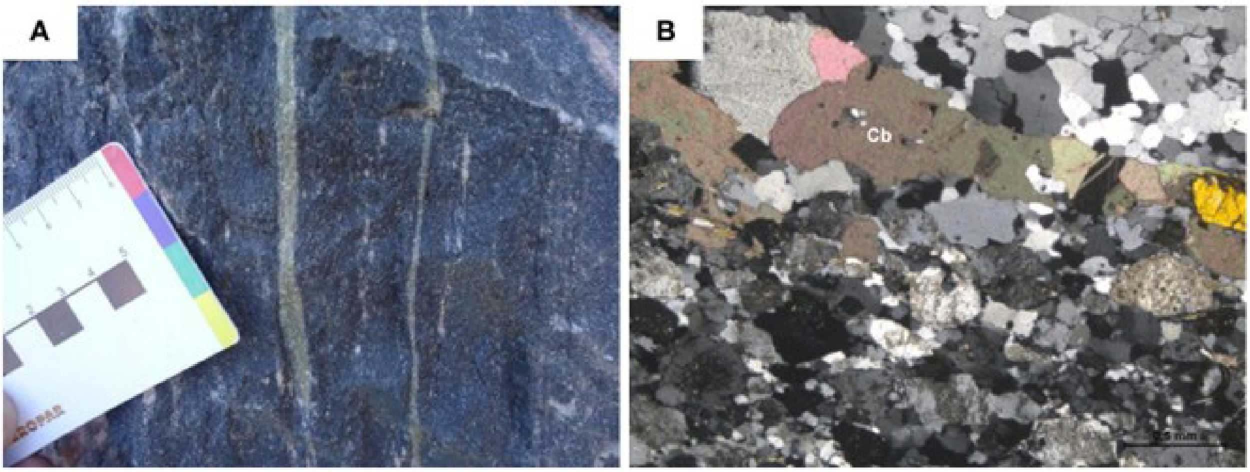

Figure 25. (A) Epidote veins, green in color and millimeter- to centimeter-thick, parallel to foliation (S_n). (B) Carbonate vein in mylonitic rock from the São Jorge quarry (cross-polarized light). Legend: Cb – carbonate.

The epidote veins (Figure 25A) are arranged parallel or discordant to the foliation (S_n). They are green in color and millimeter- to centimeter-thick. Carbonate veins were observed microscopically (Figure 25B). They occur parallel to the main foliation, with millimetric thickness. The grains are fine to medium, have serrated contacts, and are not oriented. They may show undulatory extinction.

4.3 Strain analysis

4.3.1 Fry method

The marking of the quartz crystal centers in the photomicrographs indicated moderate deformation by Fry's method (Table 1). The figures are found with moderate eccentricity (Figure 26A). The value strain ratio (R) in the XZ plane is 1.984. In the YZ plane, the measurement is lower, around 1.498 (Table 1).

4.3.2 Polar method

The results (Figure 26B) are moderately dispersed around the mean (red dot). They have been contoured within 25% of the density distribution. The strain ratio (R) values are 1.617 (XZ plane) and 1.558 (YZ plane). The other strain parameters can be seen in Table 2.

Table 1. Strain parameters obtained with the Fry method.

Sample 1	XZ	YZ
Number of measurements (N)	111	191
Maximum radius of ellipse or ellipsoid (A)	75.570	51.034
Intermediate radius of ellipsoid (B)	38.098	34.075
Ellipse ratio (R)	1.984	1.498
Orientation of ellipse long axis clockwise from X axis (Φ)	3.40°	6.18°

Table 2. Strain parameters obtained with the Polar method.

Sample 1	XZ	YZ
Number of measurements (N)	32	44
Ellipse ratio (R)	1.617	1.558
Orientation of ellipse long axis clockwise from X axis (Φ)	56.47°	18.28°

4.3.3 Rf/ϕ method

The values present in the XZ plane are more dispersed around the mean than the YZ plane data (Figure 26C). The R values are 1.967 (XZ plane) and 2.089 (YZ plane). The mean is represented in red, and the data has been contoured by 25% of the density distribution. The strain parameters are presented in Table 3.

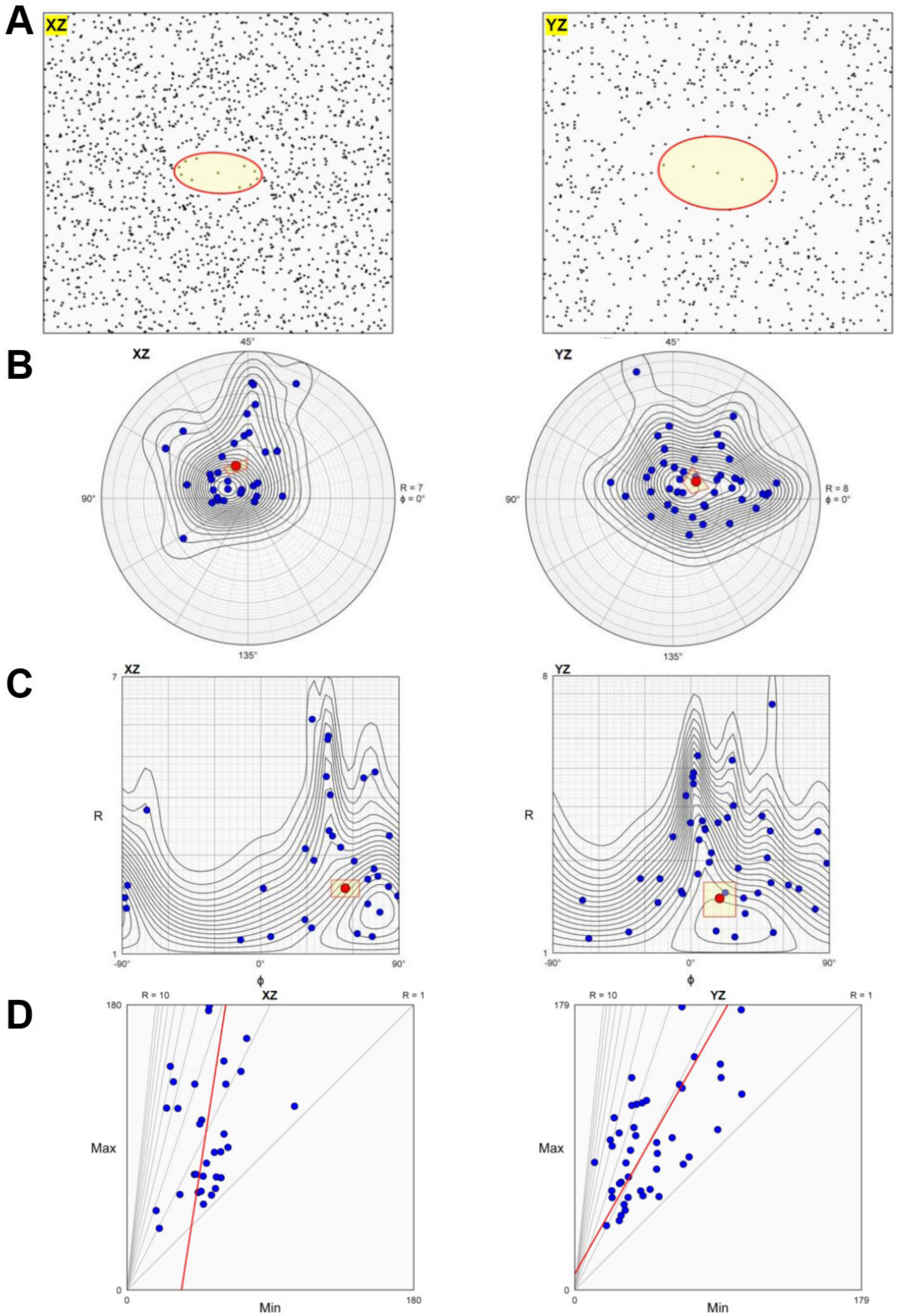

Figure 26. (A) Fry method applied to the mylonitic stromatic metatexite from the São Jorge quarry. (B) Polar method applied to the mylonitic stromatic metatexite from the São Jorge quarry. The mean is represented in red. |(C) Rf/ϕ method applied to the mylonitic stromatic metatexite from the São Jorge quarry. (D) Cloos plot of axial ratios applied to the mylonitic stromatic metatexite from the São Jorge quarry. The red line is the least squares best-fit solution.

4.3.4 Cloos plot

To determine axial ratios and orientations of the strain ellipsoids (C/A = Min/Max) the method of Cloos (1971) was used. The plot shows a best-fit solution for the data ratio (line in red; Figure 26D). In the XZ plane, the R-value equals 6.4869 and in the YZ plane, the R number is 1.7686. The strain parameters are seen in Table 4 and the graphs in Figure 26D.

4.3.5 Flinn diagram

For the São Jorge quarry sample, results from the Fry, Polar, and Rf/ϕ methods were used to construct the Flinn, Nadai-Hsü, and strain ellipsoid diagrams (Table 5), following the criteria of Hossack (1968). In the Flinn diagram (Figure 27A), the São Jorge quarry mylonite migmatites are in the apparent flattening field, with the formation of oblate ellipsoids and S- and SL-type tectonites. All the observed values present K<1 (Table 6).

Table 3. Strain parameters obtained with the Rf/ϕ method.

Sample 1	XZ	YZ
Number of measurements (N)	32	44
Ellipse ratio (R)	1.967	2.089
Orientation of ellipse long axis clockwise from X axis (Φ)	34.32°	17.98°

Table 4. Strain parameters obtained from the Cloos plot.

Sample 1	XZ	YZ
Number of measurements (N)	32	44
Ellipse ratio (R)	6.4869	1.7686

4.3.6 Nadai-Hsü diagram

In the plot the samples lie in the oblate ellipsoids field, generating S- and SL-type tectonites (Figure 27B). The strain parameters (ε, υ) are presented in Table 7.

4.3.7 Strain ellipsoids

The three-dimensional representation of the ellipsoid plots generated from the XZ and YZ section data is shown in Figure 27C. The data (A, B, C, D) and the strain axes collected from a two-dimensional representation for the Fry, Polar, and Rf/ϕ methods can be seen in Table 8.

4.3.8 Strain maps

The strain maps (Figure 27D) present the ellipsoids and points traced in the photomicrographs used during the work. They occur heterogeneously distributed in the two sections, with a predominance of ellipsoids in the NW-SE direction. The XZ plane shows a concentration of ellipsoids in the southern portion of the map and the YZ plane shows a concentration of ellipsoids in the northern part of the map. The points are similarly and homogeneously distributed on the two maps. The values related to the points and ellipsoids arrangement can be seen in Tables 9 and 10, respectively.

Table 5. Strain parameters used for the construction of the Flinn and Nadai-Hsü diagrams.

FRY PLOT				POLAR PLOT			Rf/ϕ PLOT		
N	A	B	C	A	B	C	A	B	C
1	1.984	1.498	1	1.617	1.558	1	1.967	2.089	1

Legend: A, B, and C - ellipsoid axes. N - sample number.

Table 6. Values (A/B, B/C, K) obtained from the Flinn method.

Methods	A/B	B/C	K
Fry	1.33	1.50	0.70
Polar	1.04	1.56	0.09
Rf/ϕ	1.07	1.96	0.10

Table 7. Values (ε, υ) obtained from the Nadai-Hsü method.

Methods	ε	υ
Fry	0.50	0.19
Polar	0.39	0.87
Rf/ϕ	0.60	0.80

Table 8. Ellipsoid axes (A, B, C, D) with their respective strain axes (X, Y, Z).

Methods	A	B	C	D
	X/Y/Z	X/Y/Z	X/Y/Z	X/Y/Z
Fry	-1.00/0.00/0.07	1.00/0.00/0.07	0.00/0.76/0.66	0.00/-0.76/0.66
Polar	-0.99/0.00/0.11	0.99/0.00/0.11	0.00/0.96/0.28	0.00/-0.96/0.28
Rf/ϕ	-0.94/0.00/0.34	0.94/0.00/0.34	0.00/1.00/0.13	0.00/-1.00/0.13

Table 9. Distribution of the points on the strain maps.

XZ		YZ	
Axis X	Axis Y	Axis X	Axis Y
403.73 – 2526.74	257.58 – 1421.64	263.59 – 3032.41	9.61 – 1815.65

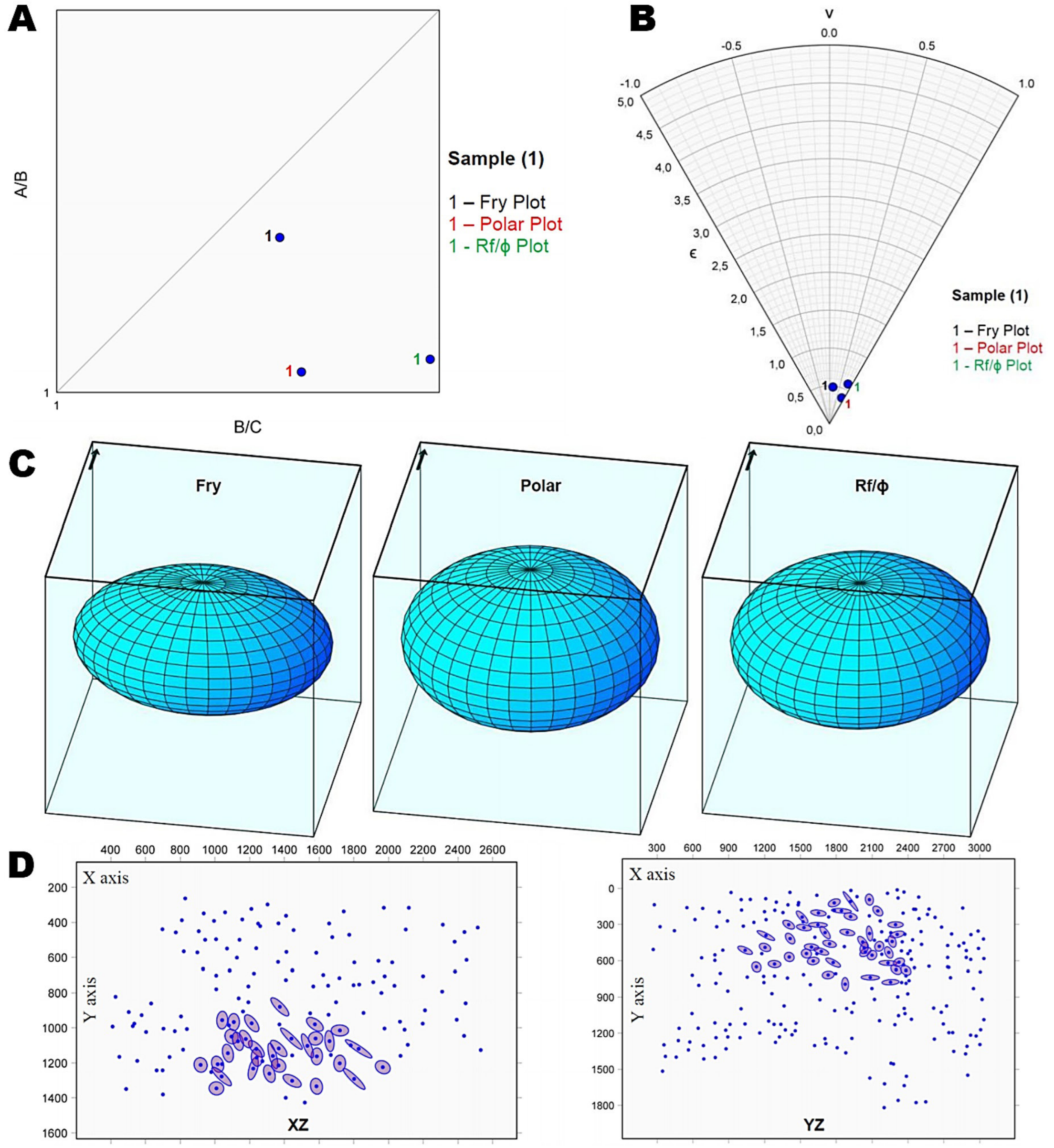

Figure 27. (A) Flinn diagram applied to the mylonitic rock from the São Jorge quarry. (B) Nadai-Hsü diagram for the mylonitic rock from the São Jorge quarry. (C) Strain ellipsoid plots generated from a mylonite sample from the São Jorge quarry, using the Hossack method (Hossack, 1968). The ellipsoids are flattened, showing S- or SL-type tectonites. (D) Strain maps for the mylonite from the São Jorge quarry.

Table 10. Distribution of the ellipsoids on the strain maps.

XZ		YZ	
Axis X	**Axis Y**	**Axis X**	**Axis Y**
921.66 – 1962.66	872.94 – 1344.72	1020.54 – 2375.07	89.29 – 786.47

4.4 Preferred crystallographic orientation (PCO)

A mylonitic stromatic metatexite sample was analyzed with the EBSD technique, according to the representativeness in the quarry. The sample corresponds to phase (D_n), with the generation of the main foliation (S_n).

4.4.1 Misorientation histograms

The albite and microcline misorientation diagrams show a sharp peak at 180°, consistent with polysynthetic or Carlsbad twinning. Some analyses were automatically indexed as anorthite; however, petrographic observations indicate that this phase is not a major constituent of the rock, and these results are therefore interpreted as possible misindexing within the plagioclase solid solution. To avoid ambiguity, future analyses should ideally be supported by EDS to confirm the precise plagioclase composition. Peaks between 5° and 10° indicate undulatory extinction and subgrain formation, whereas frequencies between 10° and 20° suggest the nucleation of new grains (Svanhnerg & Piazolo, 2010). Orientations above 20° may reflect multiple grain rotation processes or recrystallization by grain boundary migration (Ji & Mainprice, 1990). In optical microscopy, no evidence of high-temperature grain boundary migration was observed. The histograms are shown in Figures 28A, 28B, 28C.

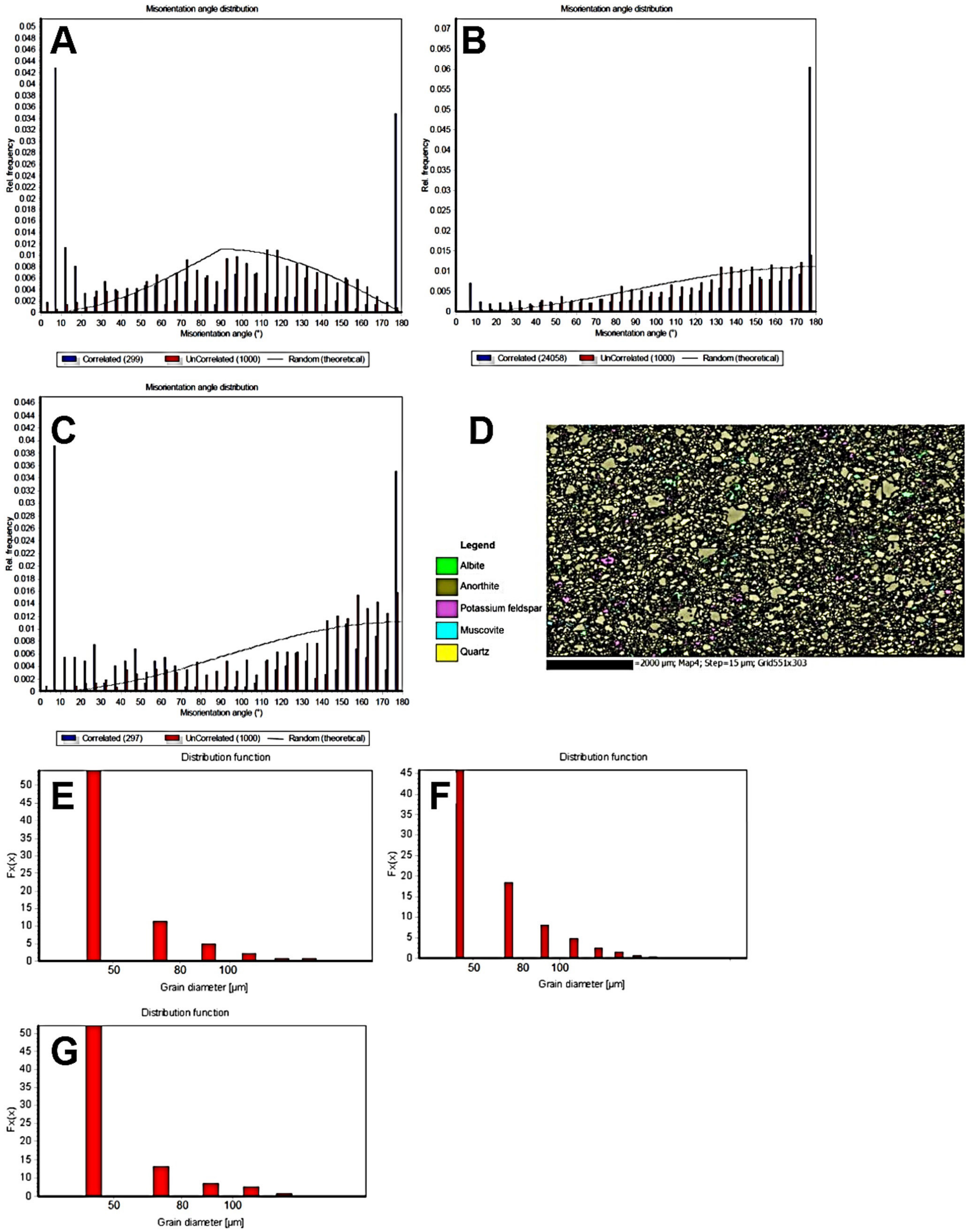

Figure 28. Misorientation histograms for albite (A), anorthite (B), and microcline (C). Phase and grain boundary map of the mylonite from the São Jorge quarry (D). Grain size distribution of albite (E), anorthite (F), and microcline (G).

4.4.2 Phase map and grain boundary

The main phases found in mylonite were albite (15%), anorthite (40%), potassium feldspar (15%), muscovite (5%), and quartz (25%). The rock has a granodioritic composition. The minerals can be flattened or elongated. The anorthite grains are fine to medium and present rectilinear, irregular, or serrated contacts. Potassium feldspar occupies the interstices between the grains and has serrated boundaries. Quartz and muscovite are very-fine to fine and show rectilinear or irregular boundaries. Albite has irregular boundaries, often resembling an ameboid appearance. The map can be seen in Figure 28D.

4.4.3 Grain size distribution

The feldspar crystals exhibit a grain diameter peak near 50 µm, with smaller peaks starting at 80 µm, occurring slightly above 100 µm (Figures 28E, 28F, 28G).

4.4.4 Band contrast map

The map provides an indication of indexing quality (Figure 29). Dark areas correspond to non-indexed regions, while light areas represent indexed portions. These show higher intensity and quality of the electron backscattered diffraction patterns (EBSP) generated during the analysis. More strongly deformed crystals display darker shades, as in the case of anorthite, which appears medium gray. Other crystals in the rock appear light gray and show lower degrees of deformation.

4.4.5 Pole figure

The crystallographic preferred orientation of albite shows (100) poles aligned with the <010> axis, which is consistent with the activation of the {100} <010> slip system. This suggests that deformation occurred by dislocation creep under moderate-temperature conditions (~500 °C; Figure 30A; Tullis & Yund 1987; Ji & Mainprice, 1990). The pole figures for anorthite and microcline show a generally random distribution (Figures 30B and 30C). In microcline, discrete maxima are noticeable between the X and Z directions.

4.4.6 Inverse pole figures

The albite diagrams (Figure 30D) in the X direction exhibit a concentration in the <010> direction. In the Y direction it shows concentrations near the <100> direction and in the Z direction it shows central maxima, between the <001> and <010> directions. Anorthite (Figure 30E) and microcline (Figure 30F) occur dispersed in the X, Y, and Z directions.

5. DISCUSSIONS

5.1 Deformation stages

The stromatic metatexites were affected by two stages of ductile deformation, generating S_{n-1} and S_n foliations, a ductile-brittle deformation phase, and a brittle deformation phase. All stages appear to be associated with tectonics in a transcurrent-transpressive regime in a progressive deformation context. Although we describe three successive deformation stages (ductile, brittle–ductile, and brittle), these are best interpreted as stages of a progressive deformation history. The overprinting relationships documented in the quarry illustrate the transition from high-temperature ductile shear to late brittle reactivation within the Curitiba Shear Zone.

5.1.1 Ductile deformation stages

S_{n-1} foliation is observed in protomylonites and occurs in a restricted manner. The surface has a low-angle dip and presents a ductile character and may be associated with the foliation of the general NW-SE direction described by Baldin et al. (2020).

The main foliation (S_n) shows general NE-SW orientation and high-angle dip to SE or NW and may be associated with the Brasiliano Cycle in the Neoproterozoic. Movement indicators suggest left-lateral kinematics for the S_n foliation, agreeing with the results of Conte (2018) and Barros et al. (2023). Features denoting the transcurrent style are foliations, S-C pairs, veins, boudins, and vertical folds, along with sub horizontal stretching lineations and positive flower structures. This style and kinematics type could explain the juxtaposition of the Atuba Complex alongside metasedimentary rocks from the Capiru Formation. In this context, the protomylonitic to ultramylonitic stromatic metatexites would be correlated to the second phase proposed by Faleiros et al., (2011), which occurred between 590-580 Ma, where the rapid exhumation of the lithotypes would be associated to a phase of transcurrent deformation. A comparable sinistral kinematic pattern was described by Conte et al. (2020) for the Atuba Complex and adjacent units of the Curitiba Terrane. Their study documented similar structural and microstructural features, including well-developed S-C fabrics, quartz ribbons, and asymmetric porphyroclasts formed under high-temperature ductile conditions. Conte et al. (2020) interpreted these features as the result of sinistral transpressional deformation during the Brasiliano Orogeny, along crustal-scale shear zones that partitioned strain across the southern Ribeira Belt. The close structural and metamorphic correspondence between the two studies suggests that the São Jorge shear zone represents a local manifestation of this broader regional sinistral system. Although the São Jorge quarry records clear evidence of sinistral shear, this kinematic pattern does not necessarily contradict the overall dextral transpressional framework proposed for the southern Ribeira Belt (Faleiros et al., 2011, 2016). As discussed by Conte et al., (2020), local sinistral shear zones within the Curitiba Terrane may reflect strain partitioning and reorientation of the principal stress axes during progressive deformation under a transpressional regime. In this context, the São Jorge shear zone can be interpreted as a localized sinistral strand developed synchronously with dextral movement along adjacent structures, both accommodating the oblique convergence that characterized the late stages of the Brasiliano Orogeny.

The Lancinha Transcurrent System defined by Fiori (1992) does not address structural aspects in the Atuba Complex, but the studies by Fassbinder (1990), Gonçalves (2012), and Cabrita (2015) corroborate the current work, recognizing the presence of this system in the Atuba Complex rocks. The Curitiba Shear Zone has N40-60E direction and is hundreds of kilometers long. It is characterized by a high-angle dip and a curvilinear map trace. In the current research, the S_n foliation was identified with a similar attitude to the Curitiba Shear Zone direction and dip.

The protomylonitic, mylonitic, and ultramylonitic portions are distinct and show recrystallization of quartz by grain boundary migration and feldspars by bulging, pointing to temperatures above 500°C (Fossen & Cavalcante 2017).

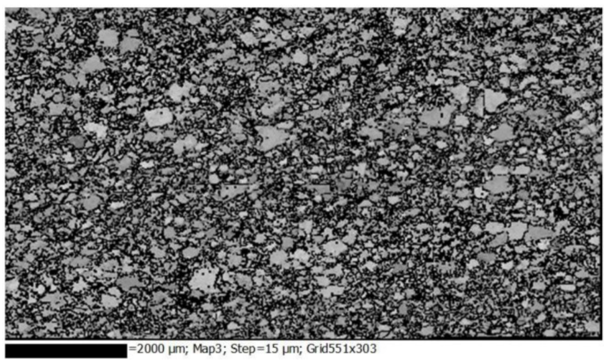

Figure 29. Band contrast map of the mylonite from the São Jorge quarry.

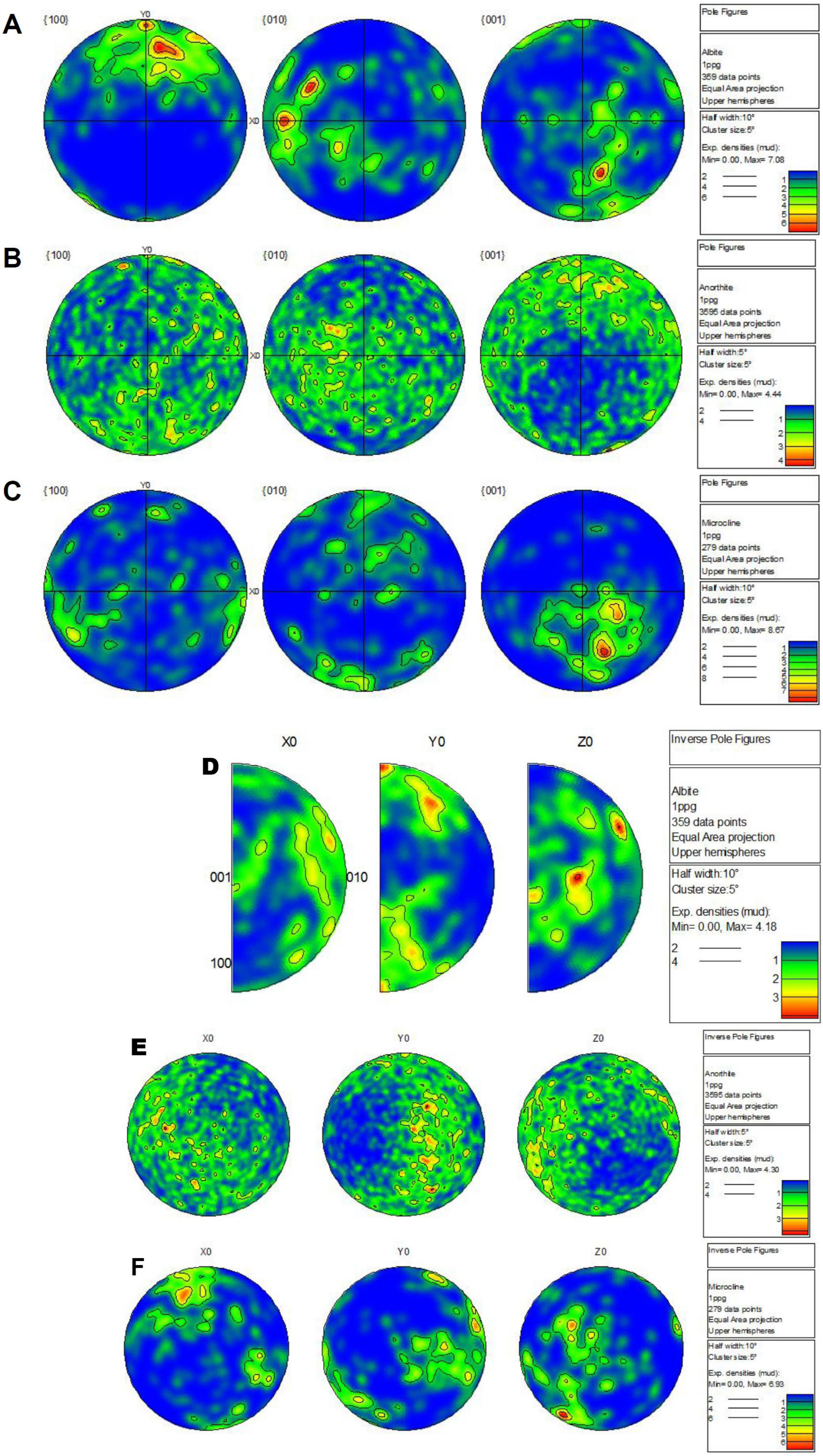

Figure 30. Pole figures for albite (A), anorthite (B), and microcline (C) crystals. Inverse pole figures for albite (D), anorthite (E), and microcline (F) crystals, according to X, Y, and Z orientations.

Deformation occurred essentially by diffusion creep mechanisms, associated with dynamic recrystallization processes.

The strain ratio (R) visualized in Fry (Table 1), Polar (Table 2), and Rf/ϕ (Table 3) methods show approximate and low values, revealing predominance of oblate ellipsoids, in the apparent flattening field. The tectonites are mainly S or SL. According to the work of Baldin et al. (2020) the R results from the São Jorge quarry in the Fry method are equivalent to 2.050-1.864 (XZ plane) and 1.962-1.217 (YZ plane). In the Polar method the R values are 1.695-1.487 in the XZ plane and 1.588-1.057 in the YZ plane. The values observed in the Rf/ϕ method are slightly larger than the other two abovementioned methods. The current work has values ranging from 1.984 to 1.498 (Fry method), 1.617 to 1.558 (Polar method), and 2.089 to 1.967 (Rf/ϕ method), corroborating with the research of Baldin et al. (2020).

The strain quantification studies developed by Kops (1994) in the Água Clara, Votuverava, and Antinha formations are like what was found in the present work. According to Kops (1994) the samples plot in the apparent flattening field, generating oblate tectonites. For Fiori (1997) the Camarinha Formation presents flattened conglomerate pebbles and occurs in the vicinity of the Lancinha Shear Zone. The R values (Rf/ϕ method) show a variation between 1.8 and 2.4, very similar to those found in the present work.

Quantitative estimates of finite strain in the Lajeado Group rocks show R values between 1.28 and 1.91, with values above 2.0 occurring locally near shear zones. In the Votuverava and Iporanga formations, strain commonly exceeded R = 2.0. In Flinn space, the ellipsoids are both prolate and oblate: the latter typically near the Ribeira and Carumbé shear zones, and the former at greater distances from them (Campanha, 2002; Faleiros, 2003). The values obtained in the present study (all ellipticities < 2.0) are comparable to those from the Lajeado Group, and indicate overall low finite strain magnitudes. At first sight, such low R values would appear incompatible with the pervasive dynamic recrystallization and intense mylonitization observed in the São Jorge quarry. However, this apparent contradiction arises because the quartz strain methods applied to mylonitic rocks do not record the total finite or bulk strain of the rock mass. Instead, they capture only the last increment of local plastic deformation recorded by the recrystallized quartz aggregates in the analyzed thin sections. In the present study, the strain markers correspond to recrystallized and dynamically deformed quartz grains, including ribbons and polygonal aggregates showing undulatory extinction, subgrain formation, and grain boundary migration - all indicative of high-temperature plastic flow (>500°C). These features are illustrated in Figures 4E-F and 14B. Consequently, the reported strain ratios (R ≈ 1.5-2.1) should be interpreted as representing the final local deformation stage of mylonitization, rather than the cumulative finite strain of the entire shear zone. Despite this limitation, the data remain a robust comparative tool for assessing relative strain variations and deformation partitioning between samples within the São Jorge quarry and across the Curitiba Shear Zone. Two factors may reconcile this apparent discrepancy. First, EBSD and strain analysis methods based on quartz grain shapes may underestimate bulk finite strain in heterogeneous, polymineralic rocks, particularly when the strain markers are not purely passive. Second, as noted by Faleiros et al. (2016), deformation in the Atuba Complex records the superposition of at least three stages. The restoration of multiple deformation increments may produce cumulative finite strains greater than those calculated in single-phase analysis, while still yielding low strain ratios in isolated domains. In this sense, the exclusively oblate ellipsoids calculated here corroborate in part the observations of Faleiros et al. (2016), although our results should be regarded as minimum estimates of strain intensity. In summary, the calculated strain ratios (R < 2) correspond to shear strains of γ < 0.7, which are apparently insufficient to explain the pervasive mylonitization observed. This reinforces that the values obtained should be interpreted as minimum estimates, constrained both by methodological limitations and by the superposition of multiple deformation stages.

The misorientation histograms display a distribution of both low- and high-angle boundaries, indicating undulatory extinction, subgrain development, and nucleation of new grains. Pole figures are generally diffuse, except for albite, which shows (100) poles aligned with the <010> axes. This pattern is consistent with activation of the {100} <010> slip system, suggesting dislocation creep at moderate temperatures (~500°C; Ji & Mainprice, 1990; Tullis & Yund, 1987). Although some EBSD points were indexed as anorthite, petrographic observations show no significant presence of this phase, and the results are therefore interpreted as possible misindexing within the plagioclase solid solution. Future studies could clarify this ambiguity by coupling EBSD with EDS analyses. Unlike most previous studies that have focused on quartz microstructures in the region (Faleiros, 2008; Cabrita, 2015; Faleiros et al., 2016; Conte, 2018), the present work specifically documents recrystallization features and crystallographic preferred orientations in feldspar.

5.1.2 Brittle-ductile and brittle deformation stages

During the brittle-ductile and brittle deformation stages, the rocks exhibit fractures, left-lateral and right-lateral fault planes, and spaced fracture cleavages, which are parallel or subparallel to the S_n foliation. In the brittle phase, left-lateral and right-lateral faults are observed in an overlapping fashion, with an abundance of right-lateral indicators over left-lateral ones. Fractures of different lengths, from millimetric to metric scale, occur and locally produce grain-size reduction interpreted as generalized comminution, characteristic of cataclastic processes. Fracturing is the predominant deformation mechanism but is accompanied by limited plastic deformation, suggested by undulatory extinction, deformation bands, subgrains, and serrated grain boundaries in quartz crystals. Evidence of widespread fracturing in quartz, feldspar, and hornblende crystals indicates that the Atuba Complex rocks most affected by brittle deformation were controlled by temperatures below 300°C (Fossen & Cavalcante, 2017). These fault-related fractures are distinguished from non-tectonic joints by the presence of kinematic indicators such as slickensides, striae, and asymmetric steps, as well as carbonate and epidote mineral fillings. Their consistent orientation parallel to the Lancinha Transcurrent System further supports their tectonic origin. Taken together, these criteria indicate that the fractures are of tectonic origin, most likely formed during the Brasiliano orogeny, although subsequent reactivation cannot be ruled out.

The Ribeira Shear Zone occurs northward of the Curitiba Shear Zone and has ENE direction. It presents quartz veins subvertical and parallel to the mylonitic foliation, with deformation features that were formed while the shear zone was active. There are folds, boudins, stretching, faults, fractures, and sub horizontal lineations consistent with transcurrent movement. Veins are abundant within the major deformation zone (Faleiros, 2003). The current work shows the same P-vein characteristics observed in Faleiros (2003) study. The veins may reveal the action of dissolution processes by pressure, metamorphic segregation, or due to the action of mobile felsic components.

The stress inversion using the Angelier & Mechler (1977) method indicates a NE–SW σ1 and a NW–SE σ3 for the left-lateral faults, and an E–W σ1 with a N–S σ3 for the right-lateral faults. These results are consistent with the orientation of the mapped fault planes and their kinematic indicators (fault striae, steps, and slickensides), which demonstrate shear displacement rather than simple opening. In addition, many of these fractures are filled with tectonically mobilized carbonates and epidote, further supporting their tectonic origin. Their systematic occurrence parallel to the Lancinha Transcurrent System (Fiori, 1992), as well as their conjugate geometry, distinguishes them from non-tectonic joints such as those produced by unloading. Thus, the fracture sets described here are interpreted as tectonic, associated with the brittle phase of the Neoproterozoic Lancinha Transcurrent System.

The retrograde metamorphism observed in the São Jorge quarry rocks is from greenschist facies, evidenced by the alteration of feldspars to sericite, the presence of epidote, biotite altered to chlorite, and hornblende altered to biotite and chlorite. This process is probably linked to the last stages of deformation of the Atuba Complex.

6. CONCLUSIONS

The São Jorge quarry is formed by protomylonitic, mylonitic, and ultramylonitic stromatic metatexites, occurring close to the Curitiba Shear Zone. These rocks correspond to the Atuba Complex, established in the Curitiba Terrane domain.

Mylonitic rocks are constituted by three stages of deformation, probably generated in a transcurrent-transpressive regime, in a context of progressive deformation. The deformation may be related to the Brasiliano Cycle during the Neoproterozoic.

The first deformation phase corresponds to ductile shear, producing mylonites with a penetrative foliation (S_n) striking NE–SW and dipping steeply to the SE or NW. Kinematic indicators consistently point to sinistral displacement. At the outcrop scale, these include sigmoidal feldspar porphyroclasts, and shear bands (S-C structures). Microscopically, asymmetric quartz–feldspar aggregates, mica fish, and quartz ribbons with internal asymmetry provide additional support for left-lateral shear. In this phase, quartz crystals exhibit lobed boundaries, indicating grain boundary migration (GBM) and temperatures above 500°C, while feldspars show undulatory extinction, subgrains, and new grains by bulging recrystallization. The deformation quantification showed low strain ratios (R) for the Fry, Polar, and Rf/ϕ methods. The ellipsoids are oblate and are found in the apparent flattening field, with the generation of S or SL tectonites. The EBSD analysis for the feldspar crystals shows poles (100) in the <010> direction for the albite, suggesting moderate temperature (500°C). For anorthite and microcline crystals, the poles are dispersed. Locally, there is a previous foliation, called S_{n-1}, defined by submillimeter to millimeter intercalations of felsic and mafic minerals, crenulate, with wavelengths and amplitude around 1 cm.

The second deformation stage is ductile-brittle, and the third stage is brittle. Both are represented by fractures, fault zones with mineral comminution, and grain size reduction. Fracturing is the main mechanism of deformation, with the aid of plastic deformation.

The retrometamorphism observed in the São Jorge quarry is noted by the alteration of feldspars, biotite, and hornblende and by the presence of epidote, indicating a late deformation phase in the Atuba Complex.

The results highlight that feldspar deformation, though often underestimated in shear zone studies, can provide critical evidence for intracrystalline plasticity and the transition from ductile to brittle regimes. The combination of strain analysis and EBSD demonstrates that the São Jorge quarry records a multiphase deformation history with left-lateral ductile shear followed by brittle–ductile and brittle right-lateral reactivation. These findings contribute to a better understanding of strain partitioning in the Atuba Complex and, more broadly, to models of transcurrent–transpressive deformation in the Ribeira Belt during the Brasiliano orogeny.

ACKNOWLEDGEMENTS

The authors express their gratitude to the Coordination for the Improvement of Higher Education Personnel (CAPES), the Federal University of Paraná (UFPR), the UFPR Geology Graduate Program, and the Laboratory of Mineral and Rock Analysis (LAMIR) for their invaluable support in the development of this research.

REFERENCES

Angelier, J., & Mechler, P. (1977). Sur une méthode graphique de recherche des contraintes principales également utilisable en tectonique et en séismologie: la méthode des dièdres droits. *Bulletin de la Société Géologique de France*, 7(6), 1309-1318. https://doi.org/10.2113/gssgfbull.S7-XIX.6.1309.

Baldin, M. T., Salamuni, E., & Lagoeiro, L. E. (2020). Quantificação da deformação em metatexitos estromáticos e rochas associadas do Complexo Atuba, Cinturão Ribeira Meridional. *Revista Geociências*, *39*(3), 631-660. https://doi.org/10.5016/geociencias.v39i03.14391.

Barros, C. E. M., Fassbinder, E., Vasconcelos, P. M., Fiori, A. P., & Bueno, N. F. S. (2023). Kinematics, recristallization mechanisms and Ar-Ar ages in Cal Shear Zone, Curitiba microplate, Central Mantiqueira Province, Brazil. *Boletim Paranaense de Geociências*, *81*, 1-26.

Basei, M. A. S., Neves, B. B. B., Siga Junior, O., Babinski, M., Pimentel, M. M., Tassinari, C. C. G., Hollanda, M. H. B., Nutman, A., & Cordani, U. G. (2010). Contribution of SHRIMP U-Pb zircon geochronology to unravelling the evolution of Brazilian Neoproterozoic fold belts. *Precambrian Research*, *183*(1), 112-144. https://doi.org/10.1016/j.precamres.2010.07.015.

Brito Neves, B. B., & Cordani, U. G. (1991). Tectonic evolution of South America during Late Proterozoic. *Precambrian Research*, *33*(1-2), 23-40. https://doi.org/10.1016/0301-9268(91)90004-T.

Brito Neves, B. B., Campos Neto, M. C., & Fuck, R. (1999). From Rodinia to Western Gondwana: an approach to the Brasiliano-Pan African cycle and orogenic collage. *Episodes*, *22*(3), 155-199. https://doi.org/10.18814/epiiugs/1999/v22i3/002.

Cabrita, D. I. G. (2015). *Análise da deformação em tectonitos do bloco sul da Zona de Cisalhamento Curitiba (PR)* (Dissertação de mestrado). Departamento de Geologia, Universidade Federal do Paraná, Curitiba.

Campanha, G. A. C. (2002). *O papel do sistema de zonas de cisalhamento transcorrentes na configuração da porção meridional da Faixa Ribeira* (Tese de livre docência). Instituto de Geociências, Universidade de São Paulo, São Paulo. https://doi.org/10.11606/T.44.2009.tde-16122009-094247.

Campanha, G. A. C., & Brito Neves, B. B. (2004). Frontal and oblique tectonics in the Brazilian Shield. *Episodes*, *27*(4), 255-259. https://doi.org/10.18814/epiiugs/2004/v27i4/003.

Campanha, G. A. C., Basei, M. A. S., Tassinari, C. C. G., Nutman, A. P., & Faleiros, F. M. (2008). Constraining the age of the Iporanga formation with SHRIMP U-Pb zircon: Implications for possible Ediacaran glaciation in the Ribeira Belt, SE Brazil. *Gondwana Research*, *13*(1), 117-125. https://doi.org/10.1016/j.gr.2007.05.010.

Campanha, G. A. C., Faleiros, F. M., Cabrita, D. I. G., Ribeiro, B. V., & Cawood, P. A. (2023). The southern Ribeira Belt in Western Gondwana: a record of a long-lived continental margin and terrane collage. *Journal of South American Earth Sciences*, *127*, 104404. https://doi.org/10.1016/j.jsames.2023.104404.

Cloos, E. (1971). *Microtectonics along the western edge of the Blue Ridge*. The Johns Hopkins Press.

Conte, T. (2018). *Mecanismos de deformação e análise quantitativa textural em rochas deformadas ao longo da Zona de Cisalhamento Lancinha e adjacências* (Dissertação de mestrado). Departamento de Geologia, Universidade Federal do Paraná.

Conte, T., Cavalcante, C., Lagoeiro, L. E., Fossen, H., & Silveira, C. S. (2020). Quartz textural analysis from an anastomosing shear zone system: implications for the tectonic evolution of the Ribeira belt, Brazil. *Journal of South American Earth Sciences*, *103*, 102750. https://doi.org/10.1016/j.jsames.2020.102750.

Elliott, D. (1970). Determination of finite strain and initial shape from deformed elliptical objects. *Geological Society of America Bulletin*, *81*(8), 2221-2236. https://doi.org/10.1130/0016-7606(1970)81[2221:DOFSAI]2.0.CO;2.

Faleiros, F. M. (2003). *Zona de Cisalhamento Ribeira: Deformação, metamorfismo e termobarometria de veios sin-tectônicos* (Dissertação de mestrado). Instituto de Geociências, Universidade de São Paulo, São Paulo. https://doi.org/10.11606/D.44.2003.tde-28092015-112134

Faleiros, F. M. (2008). *Evolução de terrenos tectono-metamórficos da serrania do Ribeira e Planalto Alto Turvo (SP, PR)* (Tese de doutorado). Instituto de Geociências, Universidade de São Paulo, São Paulo. https://doi.org/10.11606/T.44.2008.tde-02092008-113513

Faleiros, F. M., Campanha, G. A. C., Martins, L., Vlach, S. R. F., & Vasconcelos, P. M. (2011). Ediacaran high-pressure collision metamorphism and tectonics of the southern Ribeira Belt (SE Brazil): evidence for terrane accretion and dispersion during Gondwana assembly. *Precambrian Research*, *189*(3-4), 263-291. https://doi.org/10.1016/j.precamres.2011.07.013.

Faleiros, F. M., Campanha, G. A. C., Pavan, M., Almeida, V. V., Rodrigues, S. W. O., & Araujo, B. P. (2016). Short-lived polyphase deformation during crustal thickening and exhumation of a collisional orogen (Ribeira Belt, Brazil). *Journal of Structural Geology*, *93*, 106-130. https://doi.org/10.1016/j.jsg.2016.10.006.

Fassbinder, E. (1990). *Análise estrutural da Falha da Lancinha, Estado do Paraná* (Dissertação de Mestrado). Instituto de Geociências, Universidade de São Paulo, São Paulo. https://doi.org/10.11606/D.44.1990.tde-19062015-152233.

Fiori, A. P. (1985). A Falha da Lancinha no Pré-Cambriano paranaense: reflexo de uma falha profunda? *Boletim Paranaense de Geociências*, *39*, 3-14.

Fiori, A. P. (1992). Tectônica e estratigrafia do Grupo Açungui – PR. *Boletim do Instituto de Geociências – USP*, *23*, 55-74.

Fiori, A. P. (1997). *Introdução à análise da deformação*. Editora da UFPR.

Fiori, A. P., Salamuni, E., & Fassbinder, E. (1987). Geologia da região de Bateias-Bocaiúva do Sul. In *Simpósio Sul Brasileiro de Geologia* (pp. 773-787). Curitiba.

Flinn, D. (1978). Construction and computation of three-dimensional deformations. *Journal of the Geological Society*, *135*(3), 291-305. https://doi.org/10.1144/gsjgs.135.3.0291.

Fossen, H., & Cavalcante, G. C. G. (2017). Shear zones – A review. *Earth-Science Reviews*, *171*, 434-455. https://doi.org/10.1016/j.earscirev.2017.05.002.

Fry, N. (1999). Fry plots: warning about summed moments. *Journal of Structural Geology*, *21*(1), 129-134. https://doi.org/10.1016/S0191-8141(98)00093-5.

Fuck, R. A., Trein, E., & Marini, O. J. (1967). Geologia e petrografia dos migmatitos do Paraná. *Boletim Paranaense de Geociências*, *23-25*, 5-41.

Gonçalves, F. M. (2012). *Caracterização da Zona de Cisalhamento Curitiba - (PR)* (Dissertação de Mestrado). Departamento de Geologia, Universidade Federal do Paraná, Curitiba.

Heilbron, M., Pedrosa-Soares, A. C., Campos Neto, M. C., Silva, L. C., Trouw, R. A. J., & Janasi, V. A. (2004). Província Mantiqueira. In V. Mantesso-Neto, A. Bartorelli, C. R. Carneiro, & B. B. Brito-Neves (Eds.), *Geologia do Continente Sul-Americano: Evolução da obra de Fernando Flávio Marques de Almeida* (pp. 203-234). Ed. Deca.

Hossack, J. R. (1968). Pebble deformation and thrusting in the Bygdin area (Southern Norway). *Tectonophysics*, *5*(4), 315-339. https://doi.org/10.1016/0040-1951(68)90035-8.

Hsü, T. C. (1966). The characteristics of coaxial and non-coaxial strain paths. *Journal of Strain Analysis for Engineering Design*, *1*(3), 216-222. https://doi.org/10.1243/03093247V013216.

Ji, S., & Mainprice, D. (1990). Recrystallization and fabric development in plagioclase. *The Journal of Geology*, *98*(1), 65-79. https://doi.org/10.1086/629375.

Kops, P. T. (1994). *Geologia das Formações Antinha, Votuverava e Água Clara a sudeste do Complexo Granítico Três Córregos* (Dissertação de Mestrado). Instituto de Geociências e Ciências Exatas, Universidade Estadual Paulista, Rio Claro.

Le Maitre, R. W., Streckeisen, A., Zanettin, B., Le Bas, M. J., Bonin, B., & Bateman, P. (Eds.) (2008). I*gneous rocks: a classification and glossary of terms: Recommendations of the International Union of Geological Sciences Subcommission on the Systematics of Igneous Rocks*. Cambridge University Press.

Nadai, A. (1950). *Theory of flow and fracture of solids*. McGraw-Hill.

Passchier, C. W., & Trouw, R. A. J. (2005). *Microtectonics*. Springer-Verlag. https://doi.org/10.1007/3-540-29359-0.

Pavan, M., Sawyer, E. W., Moraes, R., & Faleiros, F. M. (2021). Partial melting of granodiorite: Insights from Ediacaran granulite-facies metamorphism in Southern Brazil. *Journal of Petrology*, *62*(7), 1-29. https://doi.org/10.1093/petrology/egab028.

Pierin, A. R. H., Rostirolla, S. P., Barros, C. E. M., Santos, T. B., & Romeiro, M. A. T. (2008). Análise estrutural do Complexo Gnáissico Migmatítico Costeiro em Balsa Nova – PR, através de dados de campo, laser scanner e microscopia. In *Anais do Congresso Brasileiro de Geologia*. Curitiba. SBG.

Ramsay, J. G. (1967). *Folding and fracturing of rocks*. McGraw-Hill.

Salamuni, E. (1998). *Tectônica da Bacia Sedimentar de Curitiba (PR)* (Tese de Doutorado). Instituto de Geociências e Ciências Exatas, Universidade Estadual Paulista, Rio Claro.

Saque, P. F. (2017). *Levantamento fotoaéreo via drone: estudo de caso na pedreira São Jorge* (Trabalho de Conclusão de Curso). Departamento de Geologia, Universidade Federal do Paraná, Curitiba.

Sato, K., Siga Junior, O., Nutman, A. P., Basei, M. A. S., McReath, I., & Kaulfuss, G. (2003). The Atuba Complex, Southern South American Platform: Archean components and Paleoproterozoic to Neoproterozoic Tectonothermal Events. *Gondwana Research*, *6*(2), 251-263. https://doi.org/10.1016/S1342-937X(05)70974-6.

Sawyer, E. W. (2008). *Atlas of migmatites*. NRC Research Press. https://doi.org/10.1139/9780660197876.

Siga Junior, O. (1995). *Domínios tectônicos do sudeste do Paraná e nordeste de Santa Catarina: geocronologia e evolução crustal* (Tese de Doutorado). Instituto de Geociências, Universidade de São Paulo, São Paulo. https://doi.org/10.11606/T.44.1995.tde-05112013-093542.

Siga Junior, O., Basei, M. A. S., Reis Neto, J. M., Machiavelli, A., & Harara, O. M. (1995). O Complexo Atuba: Um cinturão Paleoproterozoico intensamente retrabalhado no Neoproterozoico. *Boletim IG-USP. Série Científica*, *26*, 69-98.

Siga Junior, O., Basei, M. A. S., Sato, K., Prazeres Filho, H. J., Cury, L. F., Weber, W., Passarelli, C. R., Harara, O. M., & Reis Neto, J. M. (2003). U-Pb (Zircon) ages of metavolcanic rocks, from the Itaiacoca Group: Tectonic implications. *Boletim IG-USP. Série Científica*, *3*(1), 39-50. https://doi.org/10.5327/S1519-874X2003000100004.

Silva, P. C. S., Yamato, A. A., Vasconcelos, C. S., & Lopes Júnior, I. (1998). *Projeto Folha de Curitiba (SG-22-X-D-I): Relatório Final*. Editora.

Snoke, A. W., Tullis, J., & Todd, V. R. (1998). *Fault-related rocks: a photographic atlas*. Princeton University Press. https://doi.org/10.1515/9781400864935.

Svanhnerg, H., & Piazolo, S. (2010). The initiation of strain localisation in plagioclase-rich rocks: Insights from detailed microstructural analyses. *Journal of Structural Geology*, *32*(10), 1404-1416. https://doi.org/10.1016/j.jsg.2010.06.011.

Tullis, J., & Yund, R. A. (1987). Transition from cataclastic flow to dislocation creep of feldspars: Mechanism and microstructures. *Geology*, *15*(7), 606-609. https://doi.org/10.1130/0091-7613(1987)15<606:TFCFTD>2.0.CO;2.

Vollmer, F. W. (2018). Automatic contouring of geologic fabric and finite strain data on the unit hyperboloid. *Computers & Geosciences*, *115*, 134-142. https://doi.org/10.1016/j.cageo.2018.03.006.

ARTICLE INFORMATION

Manuscript ID: BJGEO-2025-0026.R3. Received on: 1 APR 2025. Approved on: 16 DEC 2025.

How to cite: Baldin, M. T., Salamuni, E., Faleiros, F. M., Lagoeiro, L. E., Sanches, E., & Meneguzzo, I. S. Petrographic, structural, and deformational analysis in the Curitiba Shear Zone, Ribeira Belt: a case study at São Jorge quarry, Eastern Paraná State, Brazil. Braz. J. Geol. (2026), 56:e20250026. https://doi.org/10.1590/2317-4889/e20250026

MTB: Conceptualization, Data curation, Formal analysis, Investigation, Methodology, Project administration, Writing – original draft, Writing – review & editing. ES: Supervision. FMF: Supervision. LEL: Supervision. ES: Visualization. ISM: Visualization.

Conflict of interest: The authors declare that there is no conflict of interest.

Financial support: Coordination for the Improvement of Higher. Education Personnel (CAPES). Federal University of Paraná (UFPR). UFPR Geology Graduate Program. Laboratory of Mineral and Rock Analysis (LAMIR)

Data availability statement: The manuscript does not use any dataset. Therefore, no data are available for consultation.

SCIENTIFIC EDITOR: Carlos Henrique Grohmann
ASSOCIATE EDITOR: Haakon Fossen